Journal of Medicinal Chemistry

Article

Development of Novel PET Probes for Central 2-Amino-3-(3-hydroxy-5-methyl-4-isoxazolyl)propionic acid (AMPA) Receptors

Norihito Oi, Masaki Tokunaga, Michiyuki Suzuki, Yuji Nagai, Yosuke Nakatani, Noboru Yamamoto, Jun Maeda, Takafumi Minamimoto, Ming-Rong Zhang, Tetsuya Suhara, and Makoto Higuchi

J. Med. Chem., **Just Accepted Manuscript** • DOI: 10.1021/acs.jmedchem.5b00712 • Publication Date (Web): 15 Oct 2015

Just Accepted

ACS Publications

Journal of Medicinal Chemistry is published by the American Chemical Society. 1155 Sixteenth Street N.W., Washington, DC 20036

Development of Novel PET Probes for Central 2-Amino-3-(3-hydroxy-5-methyl-4-isoxazolyl)propionic acid (AMPA) Receptors

Norihito Oi,[†,‡] *Masaki Tokunaga,*[‡] *Michiyuki Suzuki,*[†,‡] *Yuji Nagai,*[‡] *Yosuke Nakatani,*[†,‡] *Noboru Yamamoto,*[†] *Jun Maeda,*[‡] *Takafumi Minamimoto,*[‡] *Ming-Rong Zhang,*[‡] *Tetsuya Suhara,*[‡] *and Makoto Higuchi**[,‡]

[†]Tsukuba Research Laboratories, Eisai Co., Ltd., 5-1-3 Tokodai, Tsukuba, Ibaraki 300-2635, Japan, [‡]Molecular Imaging Center, National Institute of Radiological Sciences, 4-9-1 Anagawa, Inage-ku, Chiba, Chiba 263-8555, Japan

*To whom correspondence should be addressed: Phone: +81 43 206 4700. Fax: +81 43 253 0396. E-mail: mhiguchi@nirs.go.jp. Address: Molecular Imaging Center, National Institute of Radiological Sciences, 4-9-1 Anagawa, Inage-ku, Chiba, Chiba 263-8555, Japan.

ABSTRACT

We document the development of PET probes for central AMPA receptors and their application to in vivo imaging of animals. Initial screening of perampanel derivatives was performed to identify probe candidates. Despite the high autoradiographic contrast yielded by several radioligands, rat PET scans did not support their in vivo suitability. Further focused derivatization and second screening by ex vivo LC-MS measurements led to the selection of 2-[1-(3-methylaminophenyl)-2-oxo-5-(pyrimidin-2-yl)-1,2-dihydropyridin-3-yl]benzonitrile, **21a**, and its analogs as candidates. [^{11}C]**21a** was shown by autoradiography to specifically bind to the neocortex and hippocampus, consistent with AMPA receptor localization. PET imaging with [^{11}C]**21a** demonstrated moderate uptake of radioactivity in rat and monkey brains, with the retention of radiosignals being consistent with autoradiograms, and the uptake was blocked by pretreatment with unlabeled **21a** in a dose-dependent manner. The current approach has facilitated the discovery of a PET probe potentially suitable for translational research and development focused on AMPA receptors.

INTRODUCTION

Glutamate is the primary excitatory neurotransmitter in the brain, and it exerts its physiologic effects via interaction with two major families of receptor proteins: mGluRs and iGluRs.[1] mGluRs allow glutamate to modulate cell excitability by activating second messenger signaling pathways, while iGluRs are ligand-gated tetrameric ion channels that mediate fast synaptic responses to glutamate.[2–4] Three classes of iGluRs have been identified as AMPA, kainate, and NMDA receptors.[3] iGluRs mediate the majority of excitatory synaptic neurotransmission in CNS, and regulate synaptic plasticity underlying memory/learning and differentiation/growth of the nervous system.[5] AMPA receptors have also been implicated in excitotoxic conditions exemplified by epilepsy and ischemia,[6,7] highlighting the significance of these receptors as therapeutic targets.

Scheme 1. Chemical Structures of AMPA Receptor Antagonists

Competitive

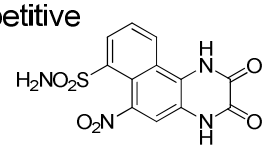

1: NBQX

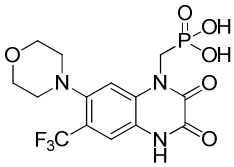

2 (Fanapanel, ZK200775)

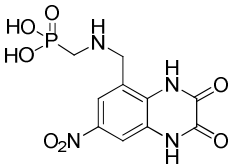

3 (Becampanel, AMP397)

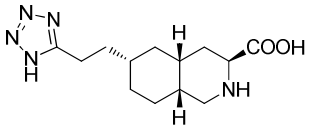

4 (Tezampanel, LY293558)

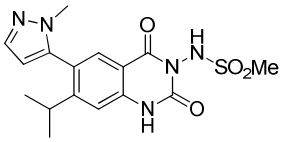

5: (Selurampanel, BGG492)

Noncompetitive

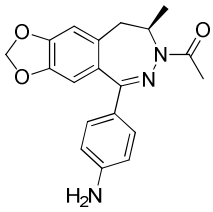

6: (Talampanel, GYKI-537773)

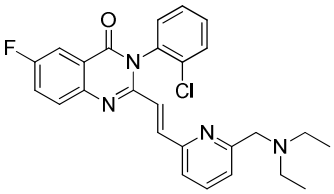

7: (CP465022)

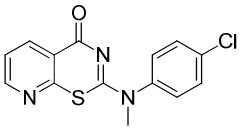

8: (YM928)

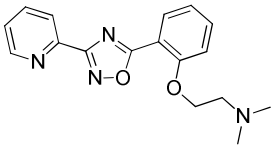

9: (Irampanel, BIIR561)

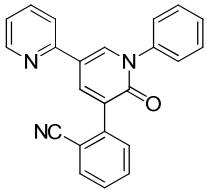

10: (Perampanel, E2007)

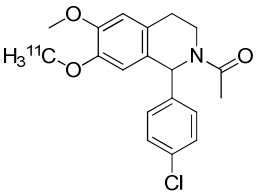

[^{11}C]**11**

The first reported competitive AMPA receptor antagonists were quinoxalinedione derivatives such as **1** (NBQX),[8] but their therapeutic utility was hampered by poor water solubility and low BBB penetration. This finding triggered further development of drugs with similar mechanism of action, including **2** (fanapanel, ZK200775),[9] **3**

(becampanel, AMP397),[10] **4** (tezampanel, LY293558), [11] and **5** (selurampanel, BGG492).[12] **3** and **5** were evaluated in clinical studies, but no competitive AMPA/kainate antagonist has so far reached the market (Scheme 1).

Meanwhile, noncompetitive AMPA receptor antagonists have actively been explored, expecting that their effectiveness will not significantly influence normal glutamatergic activity as compared with competitive antagonists.[13] A 2,3-benzodiazepine derivative, GYKI-53655, is one of the best-known compounds of this category, and **6** (talampanel, GYKI-537773) reached the Phase II clinical trial stage as an anti-epileptic agent.[14,15] Other structurally similar compounds with anticonvulsant activity, including **7** (CP465022)[16] and **8** (YM928),[17] have also been identified as noncompetitive AMPA receptor antagonists. Among additional drug candidates of this class, **9** (irampanel, BIIR561)[18] has been tested for treatment of stroke in Phase I/IIa trials, and **10** (perampanel, E2007)[19] has been approved by the US Food and Drug Administration and other regulatory agencies for treatment of epilepsy.

In vivo PET assays of central AMPA receptors and their occupancy by drugs would help to gain insights into the molecular basis of neurospychiatric disorders and to obtain proof of therapeutic concepts in clinical trials.[20-22] PET is a non-invasive, molecular imaging modality that can be used for translational development of AMPA receptor

ligands from animal models to humans. The relationship between AMPA receptor occupancy and dose or plasma concentration of a drug may allow us to clarify relevant dose settings and to minimize adverse events.

PET assessments of treatments targeting AMPA receptors require a radioprobe competing with the therapeutic agent on a binding pocket at the receptor. A small number of PET probes for AMPA receptors have been published, including *N*-acetyl-1-(4-chlorophenyl)-6-methoxy-7-[^{11}C]methoxy-1,2,3,4-tetrahydroisoquinoline ([^{11}C]**11**),[23,24] but PET studies with [^{11}C]**11** demonstrated its rapid clearance from the CNS and low specific binding in rats.[23] Several radiolabeled talampanel derivatives have been described in a patent application,[25] and radiosynthesis of [^{11}C]**10** was recently documented.[26] However, their utility as PET probes is yet to be established. In addition, transmembrane AMPA receptor regulatory proteins (TARPs) have been highlighted as one of promising drug targets.Among such drugs, LY450295 is classified as a potentiator of TARP that can label AMPA potentiator binding sites,[27,28] and [^{18}F]TARP252 has been evaluated in a clinical PET study by the National Institute of Mental Health in the United States.

Here, we report a systematic approach to the discovery of suitable radioprobes that can be used for PET imaging of AMPA receptors targeting the CNS. We identified

candidate PET probes suitable for AMPA receptor imaging from perampanel derivatives, which is our novel class of compounds with high binding affinity for this receptor. We initially radiolabeled several perampanel analogs[29-31] to determine a K_i value sufficient for producing high autoradiographic contrasts of specific binding components in a rat brain slice.A focused chemical library was then constructed from one of the initially tested compound**s** in consideration of the permeability through BBB, which was quantified in rats by cassette dosing[32] of unlabeled compounds. Subsequent evaluation of candidates by in vivo PET imaging in rats and monkeys demonstrated that a compound, **21a**, could be a potential PET probe for AMPA receptors.

RESULTS AND DISCUSSION

Workflow for Selection of PET Probe Candidates. An outline flow of our strategy for the development of AMPA receptor PET probes is provided in Supporting Information, Figure 1. We firstly selected a set of perampanel derivatives, **12a**–**20a**, from Eisai's compound library according to the presence of a possible ^{11}C radiolabeling site, and evaluated K_i values of these compounds for AMPA receptors by in vitro binding assays using rat brain homogenates. Compounds **12a**–**20a** displayed a considerable range of affinity for AMPA receptors (5 nM < K_i < 3 μM) and lipophilicity

(2 < cLogP < 5). Subsequently, radiosyntheses of **12a**–**20a** were performed, and their specific binding to AMPA receptors was evaluated by in vitro autoradiography of rat brain slices. Similar to previous reports on the development of other classes of PET probes,[33,34] a K_i value required for high-contrast autoradiographic detection of the target component was determined in this experiment. We then found that [^{11}C]**19a** and [^{11}C]**20a** exhibited relatively high affinity and clear autoradiographic contrasts for the target.

[^{11}C]**20a** yielded the highest contrast of specific binding sites in autoradiography, but the in vivo uptake of [^{11}C]**20a** into the wild-type rat brain was very low. By contrast, rat PET data demonstrated that a significant amount of [^{11}C]**19a** was transferred to the brain, but this did not produce a regional difference in radioactivity retention, implying that there was insufficient binding affinity of this compound for AMPA receptors.

Based on these findings, we constructed a small-scale focused chemical library consisting of 80 compounds derived from **20a**, and identified the second set of candidates with K_i value < 30 nM and FR < 2.0. Cassette dosing of 12 unlabeled test compounds followed by LC-MS measurements of these chemicals in tissue extracts was conducted in rats. Four compounds, **21a**–**24a**, showed moderate BBB penetration, and were selected as test chemicals for PET assays. These compounds were radiolabeled,

and were further characterized by in vitro autoradiography of brain slices and in vivo PET imaging of rats and a rhesus monkey, resulting in identification of [^{11}C]**21a** as a potential radioprobe applicable to AMPA receptor PET imaging in animals and humans.

Table 1. Pharmacological Properties of Initially Tested PET Probe Candidates

Compound	Structure	AMPA K_i (nM)	cLogP[a]	Log D[b]	Corrected P-gp FR[c] (MDR1 FR / PK1 FR)
12a	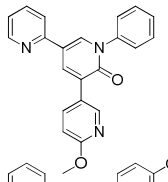	**>2670**	**4.06**	**2.19**	***d***
13a	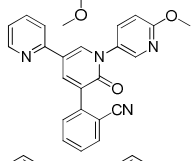	**554**	**3.85**	**2.46**	***d***
14a	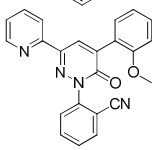	**155**	**2.56**	**3.27**	**0.7 (0.9/1.3)**
15a	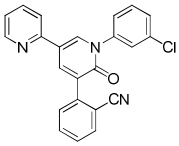	**122**	**4.93**	**1.78**	**2.2 (1.6/0.7)**
16a	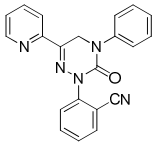	**91**	**2.52**	***d***	**0.9 (0.9/1.0)**
17a	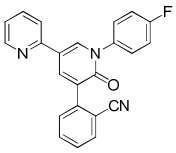	**62**	**4.36**	**1.59**	**0.9 (0.9/1.0)**
18a	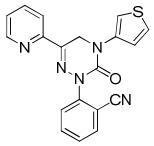	**47**	**2.17**	**2.46**	**0.9 (0.8/1.1)**
19a	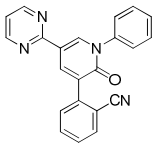	**32**	**3.20**	**1.28**	**1.2 (1.2/1.0)**
20a	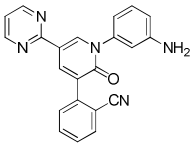	**6**	**2.48**	**1.67**	**2.8 (2.5/0.9)**

[a]cLogP value was calculated by Daylight Software ver. 4.94 (Daylight Chemical Information Systems, Inc., Niguel, CA). [b]Log *D* values were quantified in *n*-octanol/phosphate buffer (pH 7.4) by the shake-flask method (*n* = 3; maximum range, ± 5%). [c]Procedures for FR assays are provided in Experimental Section 6. [d]Not tested.

Table 2. Pharmacological Properties of PET Probe Candidates Derived From 20a

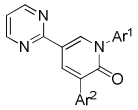

Compound	Ar^1	Ar^2	AMPA K_i (nM)	cLogP[a]	Log *D*[b]	Corrected P-gp FR[c] (MDR1 FR / PK1 FR)
20a	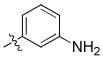		**6**	**2.48**	**1.67**	**2.8 (2.5/0.9)**
21a	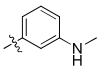		**10**	**3.24**	**2.57**	**1.9 (1.3/0.7)**
22a	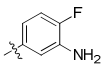		**5**	**2.59**	**1.95**	**1.7 (1.5/0.9)**
23a			**20**	**3.39**	**1.70**	**1.1 (0.9/0.8)**
24a	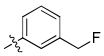		**22**	**4.03**	**2.54**	**1.1 (0.8/0.7)**

[a]cLogP value was calculated by Daylight Software ver. 4.94 (Daylight Chemical Information Systems, Inc., Niguel, CA). [b]Log *D* values were quantified in

n-octanol/phosphate buffer (pH 7.4) by the shake-flask method (n = 3; maximum range, ± 5%). [c]Procedures for FR assays are provided in Experimental Section.

Chemistry.[29–31] Compounds listed in Tables 1 and 2 and their radiosynthesis precursors were classified into three groups by their central ring structure as 2(1*H*)-pyridone, 3(2*H*)-pyridazinone, and 4,5-dihydro-1,2,4-triazin-3(2*H*)-one. Preparation of all derivatives is illustrated in Schemes 2–4.

1,3,5-Trisubstituted 2(1*H*)-pyridone derivatives were synthesized by halogenation (preferably iodination) of intermediate **26** followed by sequential couplings under modified Ullmann conditions and Suzuki-Miyaura conditions. A typical procedure is shown in Scheme 2. The introduction of substituents Ar^2 and Ar^3 to 2(1*H*)-pyridone ring was achievable, and these procedures were described elsewhere in detail.[29,30]

As radiolabeling precursors for compounds with a methoxy group, **12a**, **13a**, and **14a**, we generated hydroxy derivatives of these compounds, **12b**, **13b**, and **14b**, by cleavage of the methoxy group with acidic deprotection. Candidates with a cyano group, **15a**–**23a**, were also generated, and corresponding bromo derivatives, **15b**–**23b**, were prepared as radiolabeling precursors. Additionally, a protecting group was incorporated in an amino group of **20a**–**23a** and their precursors, **20b**–**23b**. **24a** and **24b** were readily prepared from the common starting material **24c**. A fluorinated compound, **24a**, was

directly prepared from **24c** by treatment with bis(2-methoxymethyl)aminosulfur trifluoride (BAST), and its radiolabeling precursor, **24b**, was derived from **24c** by tosylation.

Scheme 2. Syntheses of Common Trisubstituted 2-(1*H*)-Pyridone Derivatives[a]

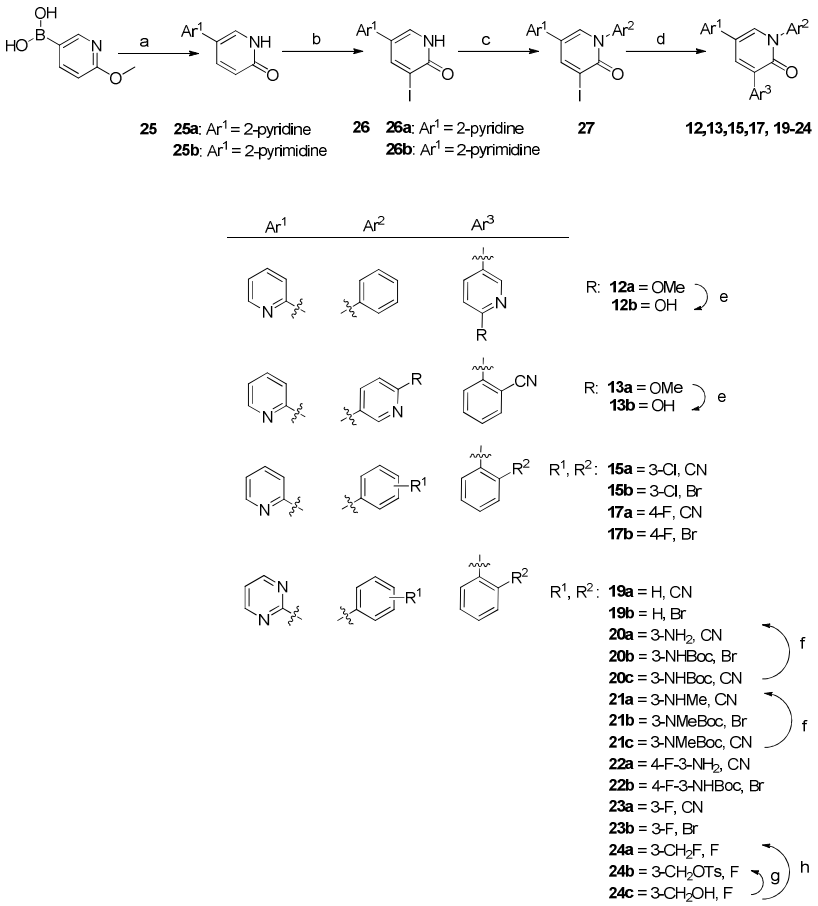

[a]Reagents and conditions: (a) i: Ar^1-Br, $Pd(OAc)_2$, PPh_3, K_2CO_3, DME–H_2O, 80°C, 1 day; ii: 4N–HCl, 80°C, 1 day; (b) NIS, $CHCl_3$, 50°C, 2 h; (c) Ar^2-boronic acid, $Cu(OAc)_2$, TEA, THF or $CHCl_3$, 60°C, 2 h; (d) Ar^3-borate or Ar^3-boronic acid,

$Pd(PPh_3)_4$, Cs_2CO_3, DMF, 110°C, 2 h; (e) BBr_3, CH_2Cl_2, rt, 0.5 h; (f) TFA, neat or CH_2Cl_2, rt, 0.5 h; (g) TsCl, TEA, CH_2Cl_2, 0°C, 1 h; (h) BAST, CH_2Cl_2, 0°C, 1 h.

Synthesis of 4,5-dihydro-1,2,4-triazin-3(2*H*)-one derivatives is outlined in Scheme 3.[31] An initial intermediate, **28**, was generated by bromination and azidation of an aromatic ring with an acetyl moiety. A secondary intermediate aminohydrazone, **29**, was obtained by condensation of **28** with aryl hydrazines, followed by reduction. Notably, triazinone ring closure resulting in **30** was afforded by modified cyclization reaction of **29** with carbodiimidazole (CDI) with high yield. Ar^2 group was then introduced to **30** by the same procedure as described in Scheme 2, leading to trisubstituted triazinones, **16b**, and **18b**. Subsequently, **16a** and **18a** were readily prepared by cyanation of **16b** and **18b**, respectively.

Scheme 3. Syntheses of Common Trisubstituted 4,5-Dihydro-1,2,4-triazin-3(2*H*)-one Derivatives[a]

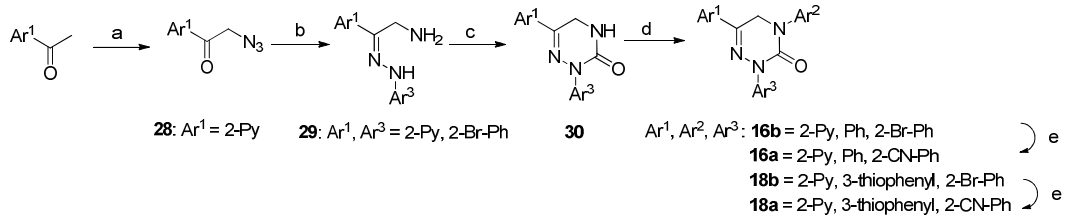

[a]Reagents and conditions: (a) i: Br_2, AcOH, 80°C, 3 h; ii: NaN_3, DMF, rt, 1 h; (b) i: Ar^3-$NHNH_2$, EtOH, rt, 1.5 h; ii: PPh_3, THF–H_2O, 80°C, 1 day; (c) i: CDI, THF, rt; ii:

toluene, reflux, 2 h; (d) Ar^2-boronic acid, $Cu(OAc)_2$, TEA, THF or $CHCl_3$, reflux, 3 h; (e) CuCN, DMF, 120°C, 1 h.

Pyridazinone derivatives were synthesized according to reaction sequences delineated in Scheme 4.[31] Condensation of 2-acetylpyridine with benzaldehyde followed by conjugate addition of cyanohydrin gave γ–ketonitrile, **31**. Compound **31** could be readily hydrolyzed, and the following treatment with methanol resulted in the generation of a common intermediate γ–ketoester, **32**. Ring formation was carried out by reaction of 2-bromophenyl hydrazine with **32** to give a compound with a 4,5-dihydro-3(2*H*)-pyridazinone ring, **33a**, which was readily oxidized to lead a compound with a 3(2*H*)-pyridazinone ring. As we used 2-bromophenyl hydrazine as an Ar^3 substituent, **33a** was easily converted to **14a** by cyanation via production of **33b**. A radiolabeling precursor, **14b**, was prepared from **14a** by treatment with BBr_3.

Scheme 4. Syntheses of Common Trisubstituted 3(2*H*)-Pyridazinone Derivatives[a]

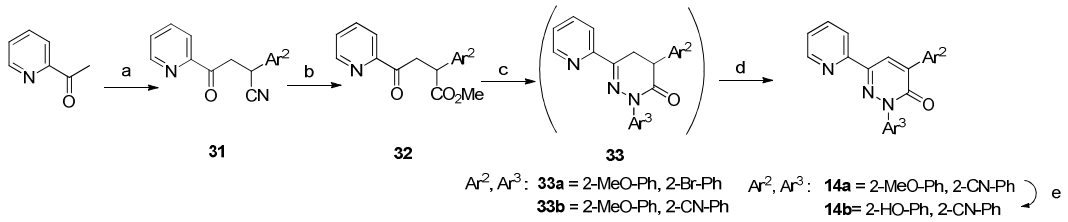

[a]Reagents and conditions: (a) i: Ar^2-CHO, KOH, MeOH:H_2O = 5:1 (v/v), 0°C, 3 h; ii: cyanohydrine, K_2CO_3, MeOH, rt, 6 h; (b) i: HCl, reflux, 8 h; ii: MeI, K_2CO_3, DMF, rt, 1 h; (c) i: Ar^3-$NHNH_2$, EtOH, rt, 3 h; ii: AcOH, reflux, 12 h; (d) CuCN, DMF, 120°C, 1 h; (e) BBr_3, CH_2Cl_2, rt, 0.5 h.

Radiosynthesis. Radiosynthesis of [^{11}C]**12a**–**23a** and [^{18}F]**24a** was performed using an automated synthesis system with various units for [^{11}C]methyliodide, [^{11}C]HCN, [^{11}C]methyltriflate, and [^{18}F]F^-. Radiosynthesis is outlined in Scheme 5.

O-[^{11}C]methyl ligands, [^{11}C]**12a**–**14a**, were prepared by reacting their precursors, **12b**–**14b**, with [^{11}C]methyl iodide ([^{11}C]CH_3I) (Scheme 5), and specific activity of the final products was 37–185 GBq/μmol at the end of synthesis (EOS).

[^{11}C]CH_3I was prepared by reducing cyclotron-produced [^{11}C]CO_2 with $LiAlH_4$, followed by iodination with 57% hydroiodic acid. For generation of [^{11}C]**12a**–**14a**, [^{11}C]CH_3I was trapped in a DMF solution containing **12b**–**14b** with an appropriate amount of base at –15°C. In [^{11}C]methylation of precursors with a 2-hydroxypyridine ring, **12b** and **13b**, *N*-methylation was the primary process, and the required *O*-[^{11}C]methylated compounds, [^{11}C]**12a** and [^{11}C]**13a**, were produced with low yield.

Compounds with a cyano substituent, [^{11}C]**15a**–**23a**, were radiolabeled by

[^{11}C]cyanation of their bromo precursors **15b–23b**. Typically, [^{11}C]CO_2 was stepwise converted to [^{11}C]HCN via [^{11}C]CH_4,[33,35] absorbed in Cu(I) solution, and reacted with **15b–23b** to give corresponding [^{11}C]cyanated derivatives. Compounds with an amino group protected by the BOC moiety, **20b–22b**, were deprotected by treatment with TFA in situ after cyanation.

[^{18}F]**24a** was obtained from **24b** by treatment with [^{18}F]F^- in the presence of K_2CO_3/ 4,7,13,16,21,24-hexaoxa-1,10-diazabicyclo[8,8,8]hexacosane (Kryptofix 222) at 85°C in CH_3CN. In this reaction, [^{18}F]F^- eluted by K_2CO_3 (66 mM) and Kryptofix 222 according to a routine procedure[36] gave [^{18}F]**24a** with a low yield (8%). By reducing the amount of K_2CO_3 to 10 mM, [^{18}F]**24a** was produced with a high yield (34%).

Scheme 5. Radiosynthesis of All Candidates[a]

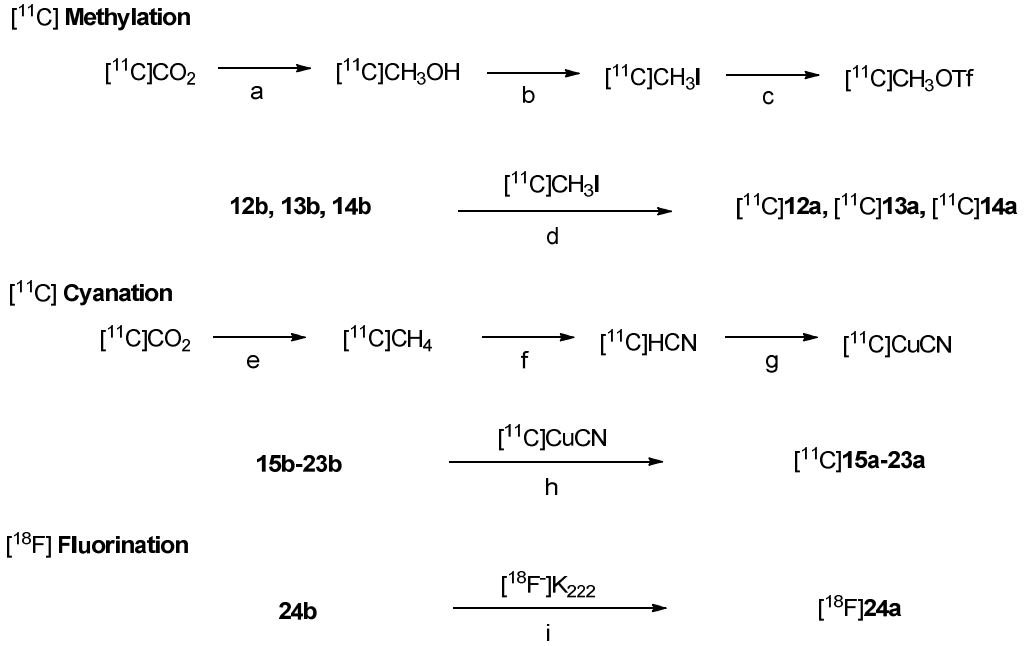

[a]Reagents and conditions: (a) $LiAlH_4$, THF, –15°C, 2 min; (b) hydroiodic acid, 180°C, 2 min; (c) AgOTf, 180°C, 1 min; (d) K_2CO_3, DMF, 50°C, 3 min; (e) H_2, Ni, 400°C, 2 min; (f) NH_3, Pt, 960°C, 2 min; (g) $Na_2S_2O_5$, $CuSO_4$, H_2O, 80°C, 2 min; (h) i: DMF, 165°C, 3 min; ii: TFA, 80°C, 2 min, in case of deprotection of BOC group; (i) K_2CO_3, CH_3CN, 85°C, 10 min.

We also labeled **21a** with ^{11}C on two distinct sites (Scheme 6)[37] to examine the metabolic profile of this compound. [^{11}C]**21a** was obtained from **20a** by treatment with [^{11}C]methyl triflate[38] in acetone at moderate yield with a trace amount of a dimethylated product. [^{11}CN]**21a** was synthesized by cyanation of **21b** and subsequent deprotection in situ by TFA. Autoradiographic and PET data in the present work were obtained by using

[^{11}C]**21a** radiolabeled on the methyl group.

Scheme 6. Two-way Radiosynthesis of 21a[a]

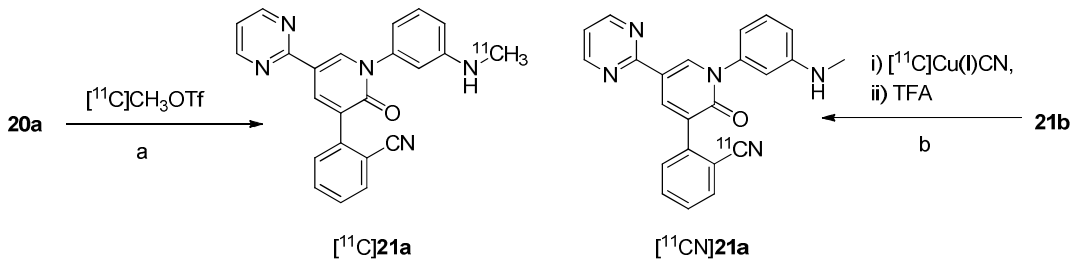

[a]Reagents and conditions: (a) acetone, rt, 1 min; (b) i: DMF, 165°C, 3 min; ii: TFA, 80°C, 2 min.

Identities of all labeled compounds were confirmed by co-injection with the corresponding unlabeled reference standard on reversed-phased analytical HPLC. Radiochemical purities of these products in the final formulation were higher than 95%. Additionally, specific activity of each product was calculated based on the UV absorption area at 254 nm using standard curves with known concentrations of unlabeled samples in a common ratio. The amount of carrier in the final product solution was measured by the same analytical HPLC. Moreover, these radioprobes did not show radiolysis at rt for 90 min after formulation, suggesting radiochemical stability over the period of at least a single PET scan.

In Vitro Autoradiography & Rat PET with Initially Selected Radioprobes. Representative in vitro autoradiographic images of sagittal rat brain sections with initially examined radiocompounds, [^{11}C]**12a**–**20a**, are displayed in Figure 1. Detectable specific binding of these compounds that could be abolished by addition of corresponding unlabeled compounds was primarily intensified in the cerebral cortex (CTX) and hippocampus (HIP) (red arrow heads), and was also present at varying levels in other areas including the cerebellum, in agreement with the known distribution of AMPA receptors, and the contrast of specific signals was consistent with in vitro K_i values of these compounds in receptor binding assays. K_i values approximating 100 nM or below were required for detectable autoradiographic contrast between receptor-enriched target region (i.e. CTX and HIP) and reference region with minimum receptor expression (i.e. brain stem [BS]). Notably, compounds with a pyridone ring, [^{11}C]**17a**, [^{11}C]**19a**, and [^{11}C]**20a**, yielded higher contrasts than triazinone ring derivatives, [^{11}C]**16a** and [^{11}C]**18a**. Another pyridine derivative, [^{11}C]**15a**, which was structurally similar to [^{11}C]**17a**, showed binding to the entire slice, presumably due to its low affinity for target receptors relative to reactivity with off-target binding components. Reactivity of a pyridazinone ring compound, [^{11}C]**14a**, with AMPA receptors was not

sufficient for conceiving this pharmacophore to be of realistic utility. Compound [^{11}C]**20a** presented the highest affinity (K_i = 6 nM) and autoradiographic contrast among the series of chemicals listed in Table 1, indicating its potential applicability to in vivo PET studies.

In vivo performance of [^{11}C]**20a** as an AMPA receptor probe was accordingly evaluated by PET scans of rat brains. There was only minimal uptake of radioactivity in the brains of wild-type rats (Figure 2B), precluding in vivo assessments of specific radioprobe binding. We postulated that a relatively high FR value of **20a** (FR = 2.8; see Table 1) accounted for its insufficient entry to the brain. P-gp–knockout rats were then employed for PET scans with this probe, and notably high retention of radioactivity in AMPA receptor-rich brain regions such as HIP and CTX versus BS was observed in these animals (Figure 2A, C). Compared to wild-type controls, an increase in radioactivity uptake was also observed in peripheral organs of P-gp–knockout animals, presumably because due to the lack of P-gp-mediated excretion of the radioprobe into urine, bile and intestinal lumen. Additional PET scans were conducted using [^{11}C]**20a** in a mouse doubly deficient in P-gp and breast cancer resistance protein (BCRP). Peak radioprobe uptake in these mice was nearly doubled as compared to wild-type mice (Supporting Information, Figure 3), and this combined genetic effect did not exceed the

impact of single P-gp deficiency in rats, implying that there was no overt contribution of BCRP to the efflux of [^{11}C]**20a** from the brain. We also conducted a supplementary PET experiment with [^{11}C]**19a** (Supporting Information, Figure 2) in wild-type rats, and brain uptake of this probe was much higher than that of [^{11}C]**20a** (Figure 2), in agreement with its FR value (FR = 1.2; see Table 1). However, [^{11}C]**19a** gave no regional difference in radioactivity, providing further evidence that an in vitro K_i value around 10 nM or below is required for detecting AMPA receptors.

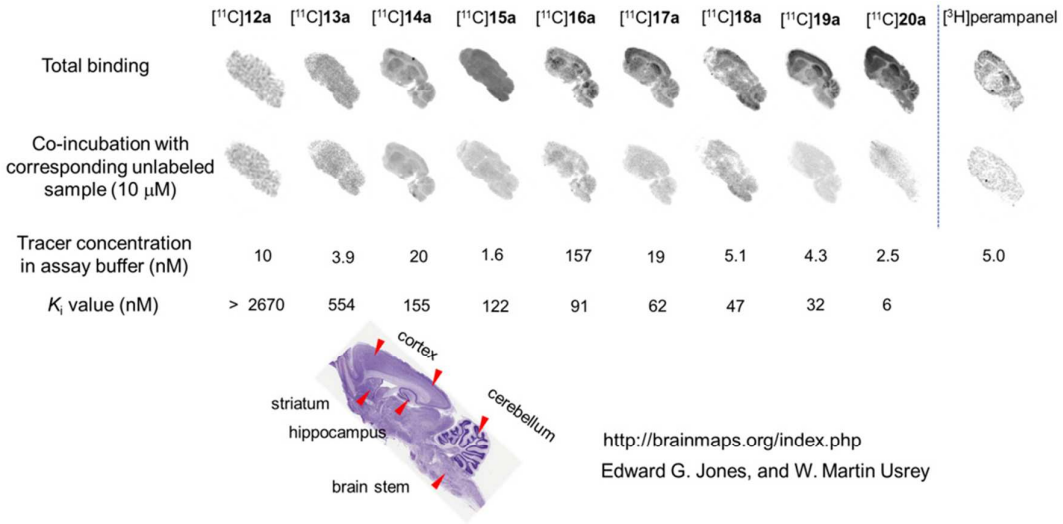

Figure 1. Representative in vitro autoradiographic images of rat brain sections reacted with initially selected radioprobes, [^{11}C]**12a**–**20a**, in the absence (total binding; upper radiographs) and presence (nonspecific binding; lower radiographs) of 10 μM of corresponding unlabeled compounds. All sagittal slices as illustrated in Nissl-stained

brain atlas were collected approximately 2.0 mm lateral to the midline, and are aligned from left to right in descending order of K_i values for AMPA receptors. Distribution of AMPA receptors is also indicated by displaying an autoradiogram with a reference radioprobe, [^{3}H]perampanel.

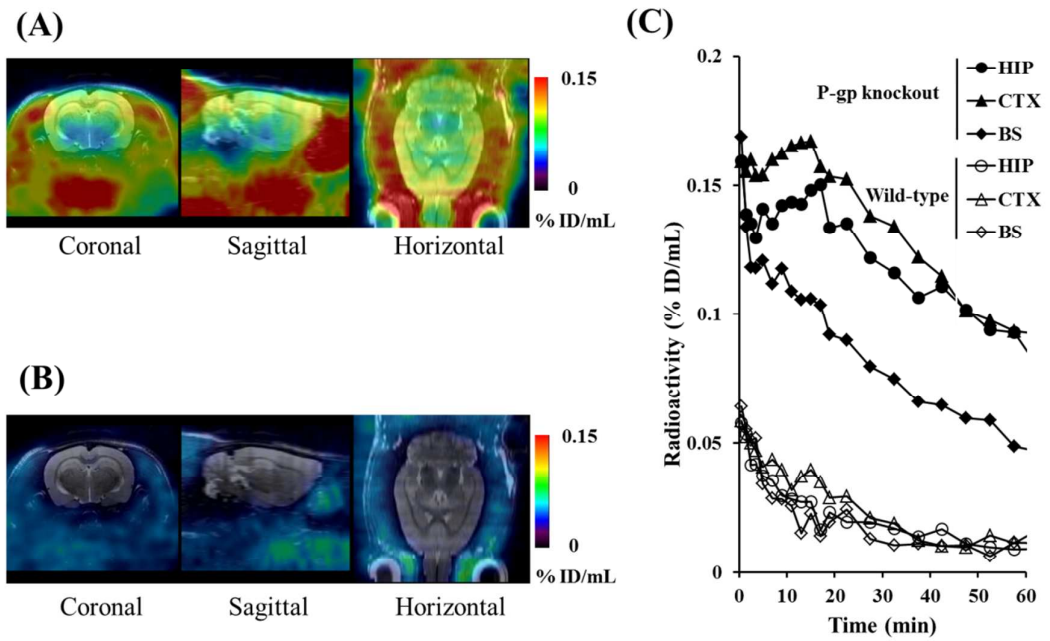

Figure 2. [^{11}C]**20a**-PET imaging of rat brains. (A, B) Representative orthogonal PET images of P-gp–knockout (A) and wild-type (B) rat brains generated by averaging dynamic data at 0–60 min after intravenous injection of [^{11}C]**20a**. PET images are superimposed on an MRI template. (C) Time–activity curves (TACs) in CTX, HIP, and BS of P-gp–knockout and wild-type rat brains after injection of [^{11}C]**20a**. Radioactivity is expressed as a percentage of injected radioligand dose per unit volume of tissue (%

injection dose/mL; %ID/mL).

Cassette Dosing Study. Twelve compounds derived from **20a** were evaluated by cassette dosing to rats in order to investigate their transfer to the brain. These compounds were selected according to the in vitro criteria for affinity (K_i value < 30 nM) and potential trans-BBB permeability (FR < 2.0), and were divided into three test groups. Each group was composed of compounds with different molecular weights, and standard curves of these compounds were obtained by LC-MS in advance to ex vivo quantification. A cocktail of four compounds was prepared and intravenously administered to rats, followed by a collection of the brains at 5, 30, 60 min after compound injection. Supernatants after centrifugation of brain homogenates were deproteinized and used for quantification of intact peaks corresponding to test compounds by LC-MS. We chose four compounds, **21a**–**24a**, with acceptable in vitro K_i value and concentration in the brain achieved at 5 min after injection for subsequent autoradiographic and PET studies (Table 3). In this evaluation, we selected compounds with a ratio of brain uptake (%ID/mL) to K_i (μM) exceeding 5.0 for the following PET evaluation. Overall, FR values of the compounds were correlated with their ex vivo brain concentrations, but did not necessarily predict the efficacy of their transfer to the

brain.

Table 3. Concentration of Compounds Quantified by Cassette Dosing

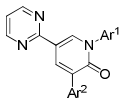

Compound	Ar^1	Ar^2	AMPA K_i (nM)	Corrected P-gp FR (MDR1 FR / PK1 FR)	Cassette dosing[a] Drug concentration in brain (%ID/mL)
20a			**6**	**2.8 (2.5/0.9)**	**(0.030)[b]**
21a			**10**	**1.9 (1.3/0.7)**	**0.077**
22a			**5**	**1.7 (1.5/0.9)**	**0.040**
23a			**20**	**1.1 (0.9/0.8)**	**0.098**
24a			**22**	**1.1 (0.8/0.7)**	**0.135**

[a]A cocktail of 50 μg/kg of four compounds in each of three groups was administered intravenously to Sprague-Dawley (SD) rats (n = 2, duplicate). Concentrations of the compounds in brain homogenates at 5 min after injection were calculated as % injection dose (%ID) by LC-MS. [b]Peak neocortical uptake at 5 min after intravenous injection of [^{11}C]**20a** in PET scans of wild-type rats is displayed as reference.

Autoradiography & Rat PET with Focused Library Compounds Derived from 20a. We autoradiographically analyzed the second set of radiolabeled compounds, [^{11}C]**21a**–**23a** and [^{18}F]**24a**, which were derived from **20a** and were selected by LC-MS measurements of cassette-dosed compounds. As illustrated in Figure 3, [^{11}C]**21a**–**23a** produced a high contrast of CTX and HIP versus BS in rat brain slices similar to [^{11}C]**20a**, and radiolabeling in other brain regions was also consistent with known AMPA receptor distribution. In contrast, autoradiographic signals yielded by [^{18}F]**24a** were mostly unrelated to the distribution of AMPA receptors, indicating substantial nonspecific binding possibly arising from the high lipophilicity of the compound. Autoradiographic binding of these radioprobes was also assessed in rhesus monkey brain slices (Supporting Information, Figure 4). [^{11}C]**20a**–**23a** exhibited abundant specific binding in CTX and HIP in a manner similar to the labeling of rat brains.

We next assessed the in vivo performance of these radioprobes by conducting rat PET assays. Among these chemicals, **21a** showed a K_i value for AMPA receptors comparable with **20a**, and its FR value was lower than **20a**, supporting applicability of this compound to in vivo imaging. Indeed, peak uptake of [^{11}C]**21a** into the brains of wild-type rats was nearly two-fold higher than that of [^{11}C]**20a** (compare Figures 2C and 4C). Notable retention of [^{11}C]**21a** in HIP and CTX also contrasted with the rapid

clearance of radioactivity in BS (Figure 4), in distinction from the lack of regionality in the kinetics of [^{11}C]**19a** (Supporting Information, Figure 2).

Unlike [^{11}C]**21a**, PET scans indicated that there was minimal uptake of [^{11}C]**22a** into the rat brain due to relatively low BBB penetration, which was in good agreement with the cassette dosing study (Supporting Information, Figure 5). Meanwhile, entry of [^{11}C]**23a** to the brain was even higher than the level observed in [^{11}C]**21a**-PET, but there were subtle differences in radioactivity retention between AMPA receptor-rich and reference regions (Supporting Information, Figure 6). Furthermore, PET scans of wild-type rats with [^{18}F]**24a** demonstrated its efficient transfer through BBB, followed by prompt clearance of radioactivity from all brain regions in a fashion unrelated to the localization of AMPA receptors (Supporting Information, Figure 7). This finding again supports the notion that $K_i \leq 10$ nM is a requisite for producing detectable AMPA receptor signals. It is also noteworthy that the radioactivity in the brain was gradually elevated beyond 10 min after injection of [^{18}F]**24a** (Supporting Information, Figure 7B), presumably due to spillover of radioactivity from defluorination products accumulating in the skull.

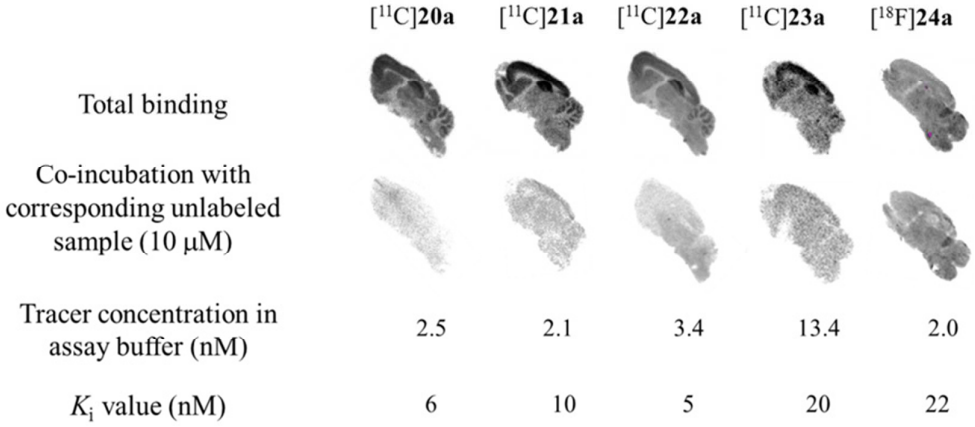

Figure 3. In vitro autoradiographic images of rat brain slices with [^{11}C]**20a** and its derivatives, [^{11}C]**21a**–**23a** and [^{18}F]**24a**. Brain sections were reacted with indicated concentrations of labeled componds in the absence (total binding; upper images) and presence (nonspecific binding; lower images) of 10 μM of corresponding unlabeled compounds. All sagittal brain slices were collected approximately 2.0 mm lateral to the midline.

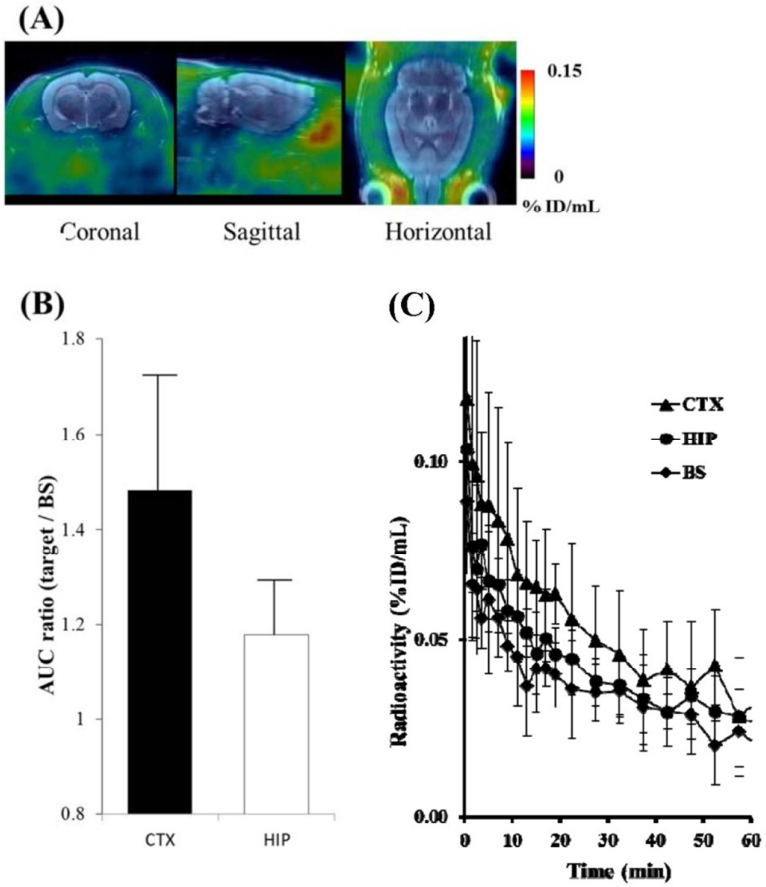

Figure 4. [^{11}C]**21a**-PET imaging of rat brains. (A) Representative orthogonal PET images of wild-type rat brain generated by averaging dynamic data at 0–90 min after intravenous injection of [^{11}C]**21a**. PET images are superimposed on an MRI template. (B) Target-to-BS ratio of AUC (0–40 min) of wild-type rat brain in CTX (closed column) and HIP (open column). (n = 3). Radioactivity is expressed as percentage of injected radioligand dose per unit volume of tissue (% ID/mL). Vertical axis begins at 0.8. (C) TACs in CTX, HIP and BS of wild-type rat brains after injection of [^{11}C]**21a**. Vertical bars in graphs represent SD.

Monkey PET. [^{11}C]**20a** and its derivatives, [^{11}C]**21a**–**23a,** were further evaluated in a PET study of a rhesus monkey.

As in rat PET assays, uptake of [^{11}C]**20a** to the monkey brain was very low (Figure 5A), while notable radioactivity was observed in PET imaging of the same monkey with [^{11}C]**21a** (Figure 5B). Moreover, retention of radioactivity in AMPA receptor-rich brain regions including CTX and HIP, in contrast with its relatively rapid clearance from BS, was observed in [^{11}C]**21a**-PET (Figure 5B, E). Radioactivity uptake to the brain of this monkey following injection of [^{11}C]**23a** was even higher than the level observed in [^{11}C]**21a**-PET, but there was only a subtle difference in radioactivity retention between AMPA receptor-rich and reference regions (Figure 5D), presumably due to insufficient affinity of [^{11}C]**23a** for the target receptor as compared with [^{11}C]**21a** (Figure 5B). Similar to [^{11}C]**20a**, [^{11}C]**22a** did not produce noticeable radioactivity in the brain (Figure 5C), despite the resemblance of the FR values of **21a** and **22a** (Table 3).

Remarkably, the order of peak radioactivity uptakes of these compounds to the monkey brain were in accordance with that of brain concentrations measured in the cassette dosing study for rats (**23a** > **21a** > **22a** > **20a**). These data justify the use of ex vivo LC-MS assays as a feasible strategy to predict entry of potential probes to the brain

when applied to PET imaging, given interspecies consistency of efflux transport systems for the test chemicals. Taking these results together, we selected [^{11}C]**21a** as a radioprobe worthy of additional characterizations.

To examine the specificity of [^{11}C]**21a** binding in rhesus monkeys, [^{11}C]**21a**-PET scans were initiated at 20 min after intravenous administration of 0.02, 0.05, and 0.1 mg/kg of unlabeled **21a**. Two monkeys were used for a series of PET scans at least two weeks apart.

TACs acquired from these monkeys demonstrated decreased differences in radioactivity retention between target (CTX and HIP) and reference (BS) regions as a function of the dose of pretreated **21a** (Figure 6A, B). Radiosignal retentions reflecting specific radioprobe binding was calculated as differences in AUC (Figure 6C, D) and ratios of AUC (Figure 6E, F) between target and reference regions were also reduced in a manner dependent on the pretreatment dose. These homologous blocking data accordingly indicate the saturability of in vivo binding of [^{11}C]**21a**.

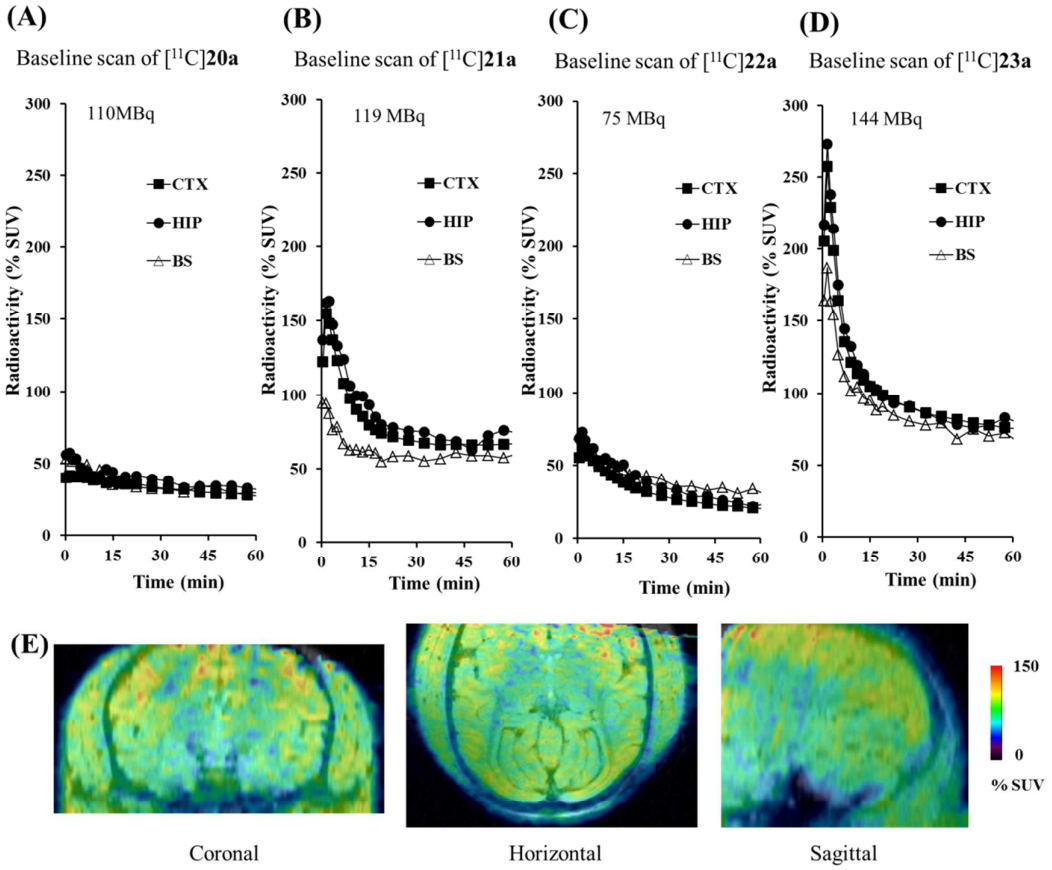

Figure 5. PET scans of a rhesus monkey with [^{11}C]**20a**–**23a**. (A-D) TACs for [^{11}C]**20a** (A), [^{11}C]**21a** (B), [^{11}C]**22a** (C), and [^{11}C]**23a** (D) in CTX (closed squares), HIP (closed circles), and BS (open triangles). Radioactivity is expressed as percentage standardized uptake value (%SUV). (E) Orthogonal PET images generated by averaging dynamic data at 0–90 min after intravenous injection of [^{11}C]**21a**. PET images are superimposed on individual MRI data.

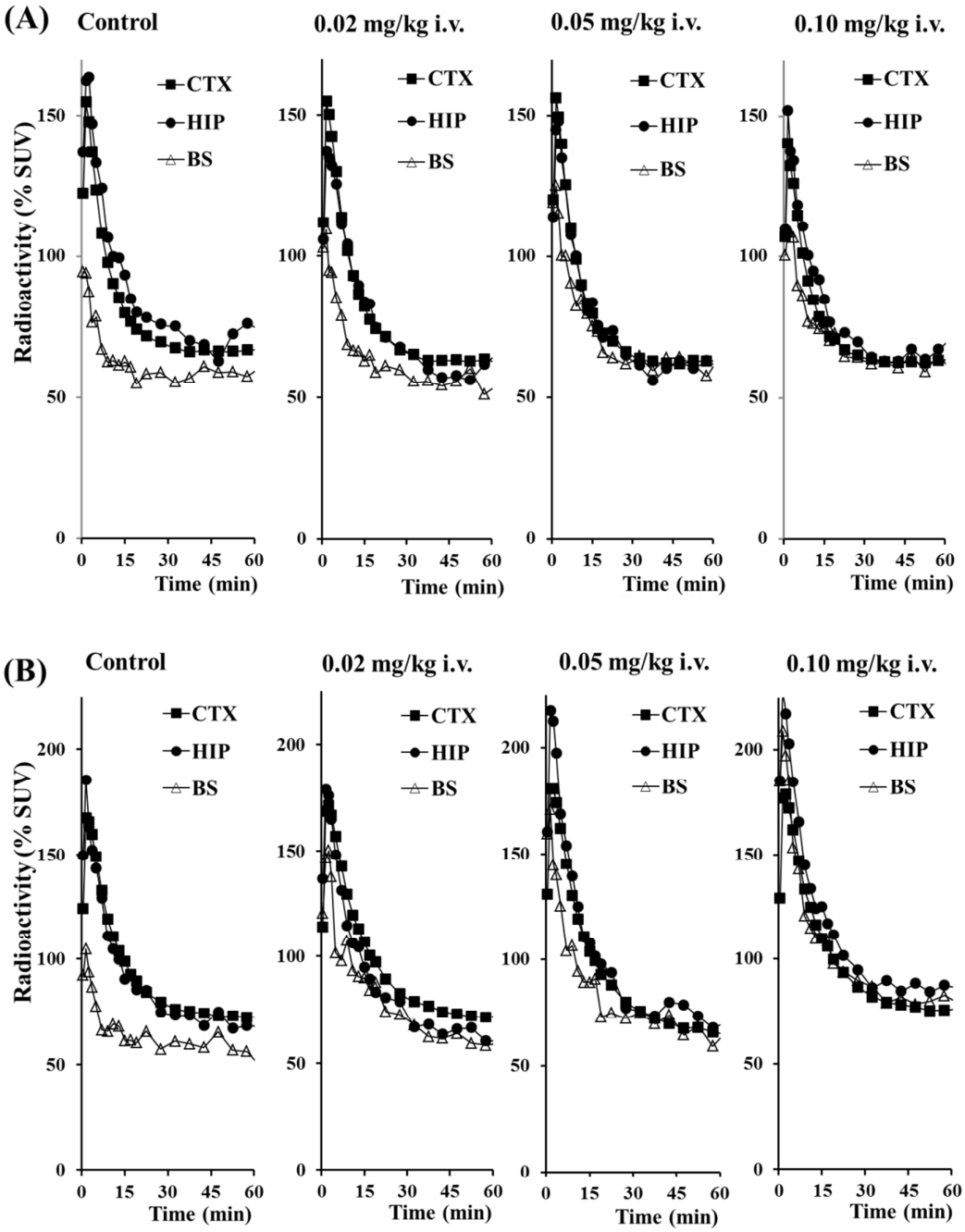
(A)
Control
0.02 mg/kg i.v.
0.05 mg/kg i.v.
0.10 mg/kg i.v.
CTX
HIP
BS
Radioactivity (% SUV)
Time (min)
(B)
Control
0.02 mg/kg i.v.
0.05 mg/kg i.v.
0.10 mg/kg i.v.
CTX
HIP
BS
Radioactivity (% SUV)
Time (min)

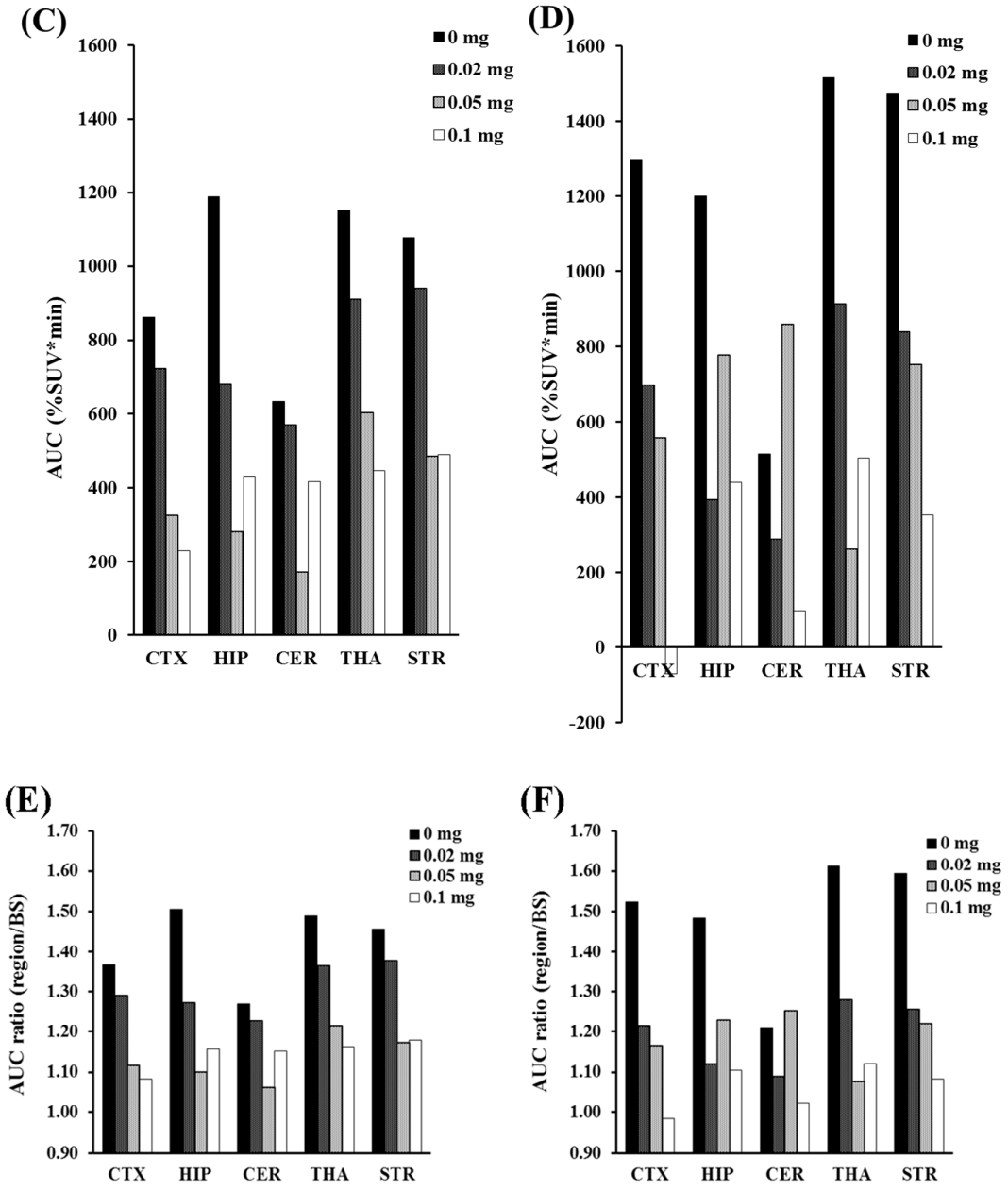

Figure 6. Homologous blocking of radioactivity retention in PET imaging of two monkeys with [^{11}C]**21a**. Unlabeled **21a** was intravenously pretreated at 20 min before radioprobe injection. (A, B) TACs for [^{11}C]**21a** in CTX, HIP, and BS of Monkeys 1 (A)

and 2 (B) at baseline and after treatment with different doses of **21a**. (C, D) Differences in AUCs between target and reference regions in Monkeys 1 (C) and 2 (D) at baseline and after treatment with various doses of **21a**. AUCs in CTX, HIP, cerebellum (CER), thalamus (THA), striatum (STR), and BS were calculated from TACs at 0–40 min, and AUC in BS was subtracted from the values in the rest of the areas. (E, F) Target-to-cerebellum ratios of AUCs calculated from TACs at 0–40 min in the baseline experiment and after treatment with different doses of **21a**.

Receptor Occupancy Measurement by Ex Vivo Rat Autoradiography with [^{11}C]21a. Compound **10** is approved in several countries for the treatment of refractory partial-onset seizures. It is reported to demonstrate significant efficacy in amygdala–kindled rats model.[39] To clarify the relationship between plasma concentration and receptor occupancy indicated by reduced radioprobe binding, the radioactivity of CTX and BS was quantified after intravenous administration of [^{11}C]**21a** with or without treatment of **10** (see Experimental Section). Receptor occupancy is estimated by measuring radioactivity ratio between CTX (region of interest) and BS (reference region), therefore the ratio approaching 1.0 with full occupancy. Our preliminary data demonstrated that total binding estimated in rat ‘a’ and rat ‘b’ approximates CTX/BS

ratio 1.3. Occupancy of receptors by **10** was indicated as reduced binding of [^{11}C]**21a** in rats 'c', 'd' and 'e', with full occupancy implied in rat 'c' by a decrease of radioactivity ratio to a value close to 1.0. Saturable binding was shown in rat 'c', presumably reaching full occupancy due to a ratio of nearly 1.0. A good correlation between CTX/BS ratio and plasma concentration of **10** was also observed in these rats. In addition, plasma concentration of **10** inducing 50% reduction of radioprobe binding was relevant to the concentration of this drug exerting pharmacological effects investigated in clinical study,[40] in consideration of species difference in plasma unbound fraction. These results supports the potential applicability of [^{11}C]**21a** to PET assays for evaluation and dose estimation of clinically relevant therapeutic agents.

Table 4. Radioactivity Ratio between CTX/BS and Plasma Concentration after Treatment with 10

Rat ID	Dose of **10** (mg/kg)	Radioactivity ratio CTX/BS	Plasma concentration (μM)
a	**0**	**1.33**	**0**
b	**0**	**1.25**	**0**
c	**10**	**1.01**	**1.62**
d	**10**	**1.14**	**0.53**
e	**10**	**1.18**	**0.44**

Reactivity of 21a with Off-target Binding Components. The pharmacological profile of **21a** was further investigated by in vitro receptor binding assays (Cerep, Poitiers, France). Reactivity of control ligands with 86 biological components including receptors, transporters, and ion channels were assayed in the absence and presence of **21a** (1 and 10 μM). **21a** did not inhibit binding of control ligands to these components by more than 50% even at high concentration (10 μM), except for A_{2A} (adenosine 2A) receptor and pBZR (peripheral benzodiazepine receptor), binding to which was reduced by 86% and 69%, respectively, by 10 μM of **21a** (see Supporting Information, Table 1). It is however unlikely that a significant portion of [^{11}C]**21a** used at much lower concentrations in autoradiographic and PET experiments reacted with these receptors. In addition, distribution of pBZR receptors[41] and A_{2A} receptors[42,43] is distinct from that of AMPA receptors, and autoradiographic binding of [^{11}C]**21a** to A_{2A} and pBZR in the neocortex was accordingly presumed to be negligible.

CONCLUSIONS

We developed novel classes of perampanel derivatives applicable to PET visualization of AMPA receptors in living brains. In our stepwise workflow, we

compared in vitro properties of non-radiolabeled test compounds with performances of their corresponding radioprobes in autoradiography and PET, and found that affinity for AMPA receptors (K_i < 10 nM), lipophilicity (2.5 < ClogP < 4.0) and reactivity with P-gp transporter (FR < 2.0) of these compounds were intimately associated with their capability as PET probes.

Indeed, **20a** exhibited high affinity for the target (K_i = 6 nM), but its relatively high reactivity with P-gp (FR = 2.8) hampered successful in vivo visualization of the targets in wild-type rats and rhesus monkeys. Our ex vivo LC-MS characterization of **20a** analogues meeting in vitro criteria (K_i < 30 nM and FR < 2.0) resulted in selection of four compounds for the second autoradiographic and PET characterizations. As FR did not fully predict transfer of the compounds through BBB as quantified ex vivo and in vivo, cassette dosing of these candidates could be a practical and handy method for determining their uptake to the brain. The validity of ex vivo LC-MS screening was demonstrated in previous literature on ligands for other targets,[32,44,45] and has been further supported in the present work by the close correlation between ex vivo LC-MS and in vivo PET measures.

We initially conceived that radioprobes with K_i value below 100 nM could produce high contrasts for AMPA receptors, according to our autoradiographic data, but [^{11}C]**19a**,

which displayed moderate reactivity with these receptors (K_i = 32 nM), failed to yield marked increase of radioactivity retention in target regions. Furthermore, noticeable signal enhancement in accordance with AMPA receptor distribution was observed in the use of [^{11}C]**21a** (K_i = 10 nM) but not [^{11}C]**23a** (K_i = 20 nM), despite sufficient trans-BBB permeability of both probes in monkeys. Hence, high-affinity compounds with K_i below 10 nM seem to be required for sensitive detection of the receptors by PET. These assessments led us to identify [^{11}C]**21a** as a radioprobe potentially suitable for preclinical and clinical PET studies. Since in vivo homologous blocking in the monkey brain and ex vivo heterologous blocking in the rat brain demonstrated dose-dependent, saturable binding of **21a**, occupancy of AMPA receptors by analogous therapeutic drugs represented by perampanel would be quantified in living subjects with [^{11}C]**21a**-PET, offering a useful index for optimization of the therapeutic dosage.

Interestingly, chemicals selected by the second-round screening (**21a** – **24a**) fulfilled most of the criteria for a PET probe candidate indicated in previous literature.[34] Both **21a** and **22a** presented a particularly high score according to these criteria, but **21a** displayed higher brain uptake than **22a** in our cassette dosing study and subsequent PET examinations. Hence, the present data support the utility of parameter-based algorithm for compound selection, while the significance of actual ex vivo and in vivo

pharmacokinetic assays has also been demonstrated.

The present PET results support the validity of [^{11}C]**21a** as an imaging agent for AMPA receptors, while there remains possibility that further improvements of chemical and pharmacokinetic properties of compounds would enable high-contrast visualization of the target molecules. This is achievable by identification of chemicals with high affinity (leading to a longer retention on the specific binding component), high brain uptake but rapid clearance from the brain with a low P-gp FR value and adequate lipophilicity, and metabolic stability in reference to the current data on **21a**.

EXPERIMENTAL SECTION

Materials and Methods. Melting points were measured using a micro melting point apparatus (MP-500P; Yanaco, Tokyo, Japan) and were uncorrected. ^{1}H-NMR spectra were recorded on a JEOL-AL-300 spectrometer (operating at 300 MHz, JOEL, Tokyo, Japan) or Varian Mercury 400 spectrometer (operating at 400 MHz, Varian, Palo Alto, CA) or Bruker Avance 600 spectrometer (operating at 600 MHz, Bruker BioSpin, Ettlingen, Germany), with tetramethylsilane as an internal standard. All chemical shifts (δ) were reported in parts per million (ppm) downfield relative to the chemical shift of

tetramethylsilane. Signals are quoted as s (singlet), d (doublet), dt (double triplet), t (triplet), q (quartet), or m (multiplet). FAB–MS and high-resolution mass spectra (HRMS) were obtained and recorded on a JEOL-AL-300 spectrometer (JEOL). ESI–MS were recorded on Thermo Fisher Scientific LTQ-Orbitrap XL spectrometer (Thermo Fisher Scientific Inc., Waltham, MA). Column chromatography was performed using Fuji Silysia BW-300 (300 mesh). Reversed-phase HPLC was performed using a JASCO HPLC module (JASCO, Tokyo, Japan) equipped with YMC Pack Pro C_{18} columns (S-5 μm, 10 mm ID ×250 mm, YMC, Kyoto, Japan) utilizing 0.1% triethylamine (TEA) in water/methanol or 0.1% TEA in water/CH_3CN for semi-separative purification. Chemical purity analysis was carried out by using YMC Pack Pro C_{18} columns (S-5 μm, 4.6 mm ID ×150 mm, YMC) with UV detector at 254 nm. In radio-HPLC purification and analysis, effluence of radio activity was monitored by NaI (Tl) scintillation detector system. All chemical reagents and solvents were purchased from commercial sources (Sigma-Aldrich, St. Louis, MO; Wako Pure Chemical Industries, Osaka, Japan; Tokyo Chemical Industries, Tokyo, Japan) and used as supplied.

Carbon-11 (^{11}C) dioxide was produced by $^{14}N(p,\alpha)^{11}C$ nuclear reactions, and $[^{18}F]F^-$ was produced by $^{18}O(p,n)^{18}F$ reaction on 95 atom% $H_2{}^{18}O$ using a CYPRIS HM-18

cyclotron (Sumitomo Heavy Industry, Tokyo, Japan). [^{18}F]F^{-} was subsequently separated from [^{18}O]H_2O using Dowex 1-X8 anion exchange resin. If not otherwise stated, radioactivity was measured with an IGC-3R Curiemeter (Aloka, Tokyo, Japan).

Chemistry. The purity of all compounds, radiolabeling precursor **17b**–**24b** and unlabeled **17a**–**24a**, was determined by an analytical HPLC method and was found to be greater than 97% for all compounds. Spectrum data of all compounds and intermediates were summarized in Supporting Information, Figure 8. Examples of typical procedures are described in the following subsections.

2-(1-(3-Aminophenyl)-2-oxo-5-(pyrimidin-2-yl)-1,2-dihydropyridin-3-yl)benzonitrile (20a). Compound **20c** (50 mg, 0.11 mmol) was dissolved in TFA (2 mL) and the mixture was stirred for 15 min at rt. The excess amount of TFA was removed in vacuo, the residue was neutralized with aqueous solution of $NaHCO_3$, extracted with ethyl acetate (AcOEt), and the extract was dried over $MgSO_4$. The organic layer was evaporated in vacuo and the residue was purified on silica gel column chromatography using *n*-heptane/AcOEt (5/5 to 0/10, v/v) to give **20a** (30 mg, 77%) as a yellowish powder; mp: 203–204°C. ^{1}H–NMR (300 MHz, $CDCl_3$, δ): 3.85 (brs, 2H), 6.76 (d, J = 9.0 Hz, 1H), 6.80–6.90 (m, 2H), 7.14 (t, J = 5.5 Hz, 1H), 7.26–7.33 (m, 1H), 7.45 (t, J = 8.1 Hz, 1H), 7.63 (t, J = 8.1 Hz, 1H), 7.69–7.80 (m, 2H), 8.65–8.73 (m, 3H), 8.75 (d, J

= 2.6 Hz, 1H). ^{13}C–NMR (150 MHz, DMSO, δ): 111.5, 111.9, 113.2, 114.0, 115.5, 118.1, 119.3, 128.6, 128.6, 129.6, 130.8, 132.9, 133.0, 138.0, 140.3, 140.6, 141.6, 149.7, 157.7 2*C, 159.6, 160.6. HRMS (FAB) calcd for $C_{22}H_{16}N_5O$, 366.1355; found, 366.1384.

***tert*-Butyl *N*-(3-(3-(2-bromophenyl)-2-oxo-5-(pyrimidin-2-yl)-1,2-dihydropyridin-1-yl)phenyl) carbamate (20b).** A mixture of the compound of **26b** (750 mg, 2.5 mmol), *N*-tert-butoxycarbonyl-3-aminophenylboronic acid (1.5 g, 6.3 mmol), copper(II) acetate (1.37 g, 7.5 mmol) and TEA (4.3 mL, 31 mmol) in THF (50 mL) was stirred at 60°C for 2 h. The reaction mixture was diluted with aqueous solution of ammonia and insoluble material was filtered out. The filtrate was extracted with ethyl acetate (AcOEt) and dried over magnesium sulfate ($MgSO_4$). The organic layer was evaporated in vacuo and the residue was purified on silica gel column chromatography using *n*-heptane/AcOEt (3/7, v/v) to give *tert*-butyl *N*-(3-(3-iodo-2-oxo-5-(pyrimidin-2-yl)-1,2-dihydropyridin-1-yl)phenyl)carbamate (470 mg, 38% yield) as a white powder; mp: 207–210°C. ^{1}H–NMR (300 MHz, $CDCl_3$) δ: 1.51 (s, 9H), 6.66 (brs, 1H), 7.09 (brd, *J* = 8.0 Hz, 1H), 7.15 (t, *J* = 4.9 Hz, 1H), 7.31 (brd, *J* = 8.0 Hz, 1H), 7.40 (t, *J* = 8.0 Hz, 1H), 7.64 (brs, 1H), 8.63 (d, *J* = 2.3 Hz, 1H),

8.69 (d, J = 4.9 Hz, 2H), 9.12 (d, J = 2.3 Hz, 1H). ESI–MS: m/z 491 (M+H), HRMS (FAB) calcd for $C_{20}H_{20}IN_4O_3$, 491.0580; found, 491.0554.

A mixture of the compound described above (150 mg, 0.31 mmol), 2-bromophenylboronic acid (184 mg, 0.92 mmol), cesium carbonate (250 mg, 0.77 mmol) and tetrakis(triphenylphosphine)palladium(0) (35 mg, 0.03 mmol) in DMF (5 mL) was stirred at 110°C for 2 h under nitrogen atmosphere. The reaction mixture was diluted with water, extracted with AcOEt, and dried over $MgSO_4$. The organic layer was evaporated in vacuo, and the residue was purified on silica gel column chromatography using *n*-heptane/AcOEt (5/5, v/v) to give the title compound (140 mg, 88% yield) as a pale brown powder; mp: 105–107°C. ^{1}H–NMR (400 MHz, $CDCl_3$, δ): 1.52 (s, 9H), 6.60 (brs, 1H), 7.13 (t, J = 4.7 Hz, 1H), 7.16–7.24 (m, 2H), 7.33–7.38 (m, 2H), 7.38–7.47 (m, 2H), 7.64–7.69 (m, 2H), 8.50 (d, J = 2.4 Hz, 1H), 8.69 (d, J = 4.7 Hz, 2H), 8.72 (d, J = 2.4 Hz, 1H). ESI–MS: m/z 519 (M+H). HRMS (FAB) calcd for $C_{26}H_{24}BrN_4O_3$, 519.1032; found, 519.1014.

***tert*-Butyl *N*-(3-(3-(2-cyanophenyl)-2-oxo-5-(pyrimidin-2-yl)-1,2-dihydropyridin-1-yl)phenyl)carbamate (20c).** According to the procedure described for the synthesis of **20b**, compound **20c** was prepared from *tert*-butyl

N-(3-(3-iodo-2-oxo-5-(pyrimidin-2-yl)-1,2-dihydropyridin-1-yl)phenyl)carbamate (225 mg, 0.45 mmol) and 2-(1,3,2-dioxaboran-2-yl)benzonitrile (258 mg, 1.35 mmol). **20c** (200 mg, 90% yield) was isolated as a yellowish powder; mp: 165°C (decomp.), 204–206°C. ^{1}H–NMR (400 MHz, $CDCl_3$, δ): 1.51 (s, 9H), 6.62 (brs, 1H), 7.13–7.20 (m, 1H), 7.14 (t, *J* = 4.8 Hz, 1H), 7.37–7.48 (m, 3H), 7.60–7.68 (m, 2H), 7.72 (d, *J* = 7.9 Hz, 1H), 7.76 (d, *J* = 7.9 Hz, 1H), 8.70 (d, *J* = 4.8 Hz, 2H), 8.71 (d, *J* = 2.6 Hz, 1H), 8.74 (d, *J* = 2.6 Hz, 1H). ESI–MS: m/z 466 (M+H). HRMS (FAB) calcd for $C_{27}H_{24}N_5O_3$, 466.1879; found, 466.1842.

2-(1-(3-(Methylamino)phenyl)-2-oxo-5-(pyrimidin-2-yl)-1,2-dihydropyridin-3-yl) benzonitrile (21a). According to the procedure described for the synthesis of **20a**, **21a** was prepared from **21c** (180 mg, 0.38 mmol). **21a** (120 mg, 85% yield) was yielded as a white powder; mp: 237-239°C. ^{1}H–NMR (400 MHz, $CDCl_3$, δ): 2.87 (brs, 3H), 3.94 (brs, 1H), 6.66–6.71 (m, 1H), 6.72 (t, *J* = 2.1 Hz, 1H), 6.80 (ddd, *J* = 0.9, 2.1, 7.9 Hz, 1H), 7.14 (t, *J* = 4.8 Hz, 1H), 7.31 (t, *J* = 7.9 Hz, 1H), 7.42–7.48 (m, 1H), 7.61–7.67 (m, 1H), 7.73–7.79 (m, 2H), 8.70–8.72 (m, 3H), 8.77 (d, *J* = 2.6 Hz, 1H). ^{13}C–NMR (150 MHz, DMSO, δ): 29.6, 109.2, 111.9, 112.1, 113.1, 115.5, 118.1, 119.3, 128.5, 128.7, 129.6, 130.8, 133.0, 133.0, 138.1, 140.3, 140.7, 141.8, 150.8, 157.7 2*C, 159.7, 160.6. ESI–MS: m/z 380 (M+H). HRMS (FAB) calcd for $C_{23}H_{18}N_5O$, 380.1511; found,

380.1517.

***tert*-Butyl (3-(3-(2-bromophenyl)-2-oxo-5-(pyrimidin-2-yl)pyridin-1(2*H*)-yl)phenyl)(methyl)carbamate (21b).** According to the procedure described for the synthesis of **21c**, **21b** was prepared from **20b** (60 mg, 1.35 mmol) by using NaH (9 mg, 60% in oil, 0.23 mmol), and iodomethane (12 μL, 0.64 mmol). **21b** (45 mg, 73% yield) was obtained as a white amorphous material. ^{1}H–NMR (400 MHz, $CDCl_3$, δ): 1.49 (s, 9H), 3.30 (s, 3H), 7.14 (t, *J* = 5.0 Hz, 1H), 7.20–7.25 (m, 1H), 7.28–7.39 (m, 3H), 7.42–7.48 (m, 3H), 7.67 (d, *J* = 8.2 Hz, 1H), 8.51 (d, *J* = 2.7 Hz, 1H), 8.69 (d, *J* = 4.8 Hz, 2H), 8.74 (d, *J* = 2.7 Hz, 1H). ESI–MS: m/z 533 (M+H). HRMS (FAB) calcd for $C_{27}H_{26}BrN_4O_3$, 533.1188; found, 533.1166.

***tert*-Butyl *N*-(3-(3-(2-cyanophenyl)-2-oxo-5-(pyrimidin-2-yl)-1,2-dihydropyridin-1-yl)phenyl)(methyl)carbamate (21c).** NaH (30 mg, 60% in oil, 0.75 mmol) was added to a solution of **20c** (200 mg, 0.43 mmol) in DMF (2 mL) at 0°C, and stirred at rt for 5 min. Iodomethane (40 μL, 0.64 mmol) was added to the reaction mixture, and stirred for 10 min. The reaction mixture was quenched with brine and extracted with AcOEt. The organic layer was dried over $MgSO_4$, and evaporated in vacuo. The residue was purified

on silica gel column chromatography using *n*-heptane/AcOEt (7/3, v/v) to give **21c** (185 mg, 90% yield) as a white amorphous material. ^{1}H–NMR (300 MHz, $CDCl_3$, δ): 1.42 (s, 9H), 3.17 (s, 3H), 7.08 (t, *J* = 4.8 Hz, 1H), 7.22–7.27 (m, 1H), 7.27–7.33 (m, 1H), 7.34–7.44 (m, 3H), 7.53–7.61 (m, 1H), 7.64 (d, *J* = 8.0 Hz, 1H), 7.70 (d, *J* = 8.0 Hz, 1H), 8.60–8.66 (m, 3H), 8.69 (d, *J* = 2.4 Hz, 1H). ESI–MS: m/z 502 (M+Na). HRMS (FAB) calcd for $C_{28}H_{26}N_5O_3$, 480.2036; found, 480.2044.

3-Iodo-5-(pyrimidin-2-yl)pyridin-2(1*H*)-one (26b). A mixture of **25b** (4.5 g, 31 mmol, see Supporting Information) and *N*-iodosuccinimide (7.0 g, 31 mmol) in $CHCl_3$ (100 mL) was refluxed for 2 h and cooled to room temperature. The reaction mixture was diluted with CH_2Cl_2 and filtered. The precipitate was washed with diethyl ether to give **26b** (6.7 g, 86% yield) as a white powder. ^{1}H–NMR (300 MHz, DMSO-d_6, δ): 7.35 (t, *J* = 4.6 Hz, 1H), 8.38 (d, *J* = 1.4 Hz, 1H), 8.81 (d, *J* = 4.6 Hz, 2H), 8.93 (d, *J* = 1.4 Hz, 1H), 12.36 (brs, 1H). ESI–MS: m/z 300 (M+H), 621 (2M+Na). HRMS (FAB): calcd for $C_9H_6IN_3O$, 299.9634; found, 299.9636.

Radiochemistry. All labeled compounds were formulated in sterile saline (3 mL) containing Tween® 80 (100 μL) and ascorbic acid (25 mg) after HPLC purification. HPLC analytical and purification conditions for all labeled compounds are shown in the Supporting Information, Figure 9. Representatives are noted here.

2-(1-(6-[^{11}C]Methoxypyridin-3-yl)-2-oxo-5-(pyridin-2-yl)-1,2-dihydropyridin-3-yl)benzonitrile ([^{11}C]13a). [^{11}C]CH_3I was synthesized from cyclotron-produced [^{11}C]CO_2 as described previously.[35] Briefly, [^{11}C]CO_2 was bubbled into 0.04 M $LiAlH_4$ in anhydrous THF (300 μL). After evaporation of THF, the remaining complex was treated with 57% hydroiodic acid (300 μL) to give [^{11}C]CH_3I, which was distilled at 180°C and transferred under N_2 gas into a solution of **13b** (1.2 mg, 2.3 μmol) and 2 M K_2CO_3 (5 μL, 2.5 μmol) in anhydrous DMF (300 μL) at rt. After the radioactivity had reached saturation, this reaction mixture was heated at 80°C for 3 min. The reaction mixture was applied to a semipreparative HPLC system. HPLC (YMC Pack Pro C_{18}) purification was completed using the mobile phase of CH_3CN/H_2O/TEA (5.0/5.0/0.01, v/v/v) at a flow rate of 5.0 mL/min. The radioactive fraction corresponding to the desired product was collected in a sterile flask, evaporated to dryness in vacuo, redissolved in 3 mL sterile saline, and passed through a 0.22 μm Millipore filter to give 0.33 GBq of [^{11}C]**13a**. The retention time (t_R) of [^{11}C]**13a** was 13.5 min for purification and 6.2 min for analysis on HPLC. The specific activity of [^{11}C]**13a** was calculated by comparison of the assayed radioactivity to the mass associated with the carrier UV peak at 254 nm. The synthesis time from end of bombardment (EOB), 33.6 min; radiochemical yield (decay-corrected), 3.7% based on [^{11}C]CO_2 (29.7 GBq);

radiochemical purity, > 99%; specific activity at end of synthesis (EOS), 17 GBq/μmol. In this reaction, ^{11}C-labeled *N*-methyl version was mainly produced in this condition as a by-product, and was eluted at 5.5 min for purification on HPLC (spectrum data were also noted in Supporting Information, Figure 9).

2-(1-(3-(Methylamino)phenyl)-2-oxo-5-(pyrimidin-2-yl)-1,2-dihydropyridin-3-yl) benzo[^{11}C]nitrile ([^{11}CN]21a). A handmade device synthesized [^{11}C]HCN in a two-step sequence of reaction. After [^{11}C]CO_2 in N_2 gas from the cyclotron was trapped at –196°C, it was heated to 50°C, moved under N_2 stream (flow rate of 10 mL/min), and mixed with H_2 gas at a flow rate of 10 mL/min. The mixed gas was passed through a Ni wire tube at 400°C in the methanizer to give a mixture of [^{11}C]CH_4 in the carrier gas. Then it was mixed with 5% NH_3 in N_2 (v/v) gas stream at a flow rate of 400 mL/min, and passed through a Pt furnace at 950°C to give [^{11}C]HCN containing gas, which was absorbed in the reaction solution via a bubbling tube until the radioactivity of the vessel reached saturation (45 s). The average of the total radioactivity recovered in the reaction vessel was about 70% based on [^{11}C]CO_2 at EOS. The synthesis of [^{11}C]**21a** from [^{11}C]HCN via [^{11}C]CuCN was successfully carried out.[33,35]

A freshly prepared solution of sodium metabisulfate (150 μL, 48 mM; 7.2 μmol) was added to a solution of copper(II) sulfate (100 μL, 44 mM; 6.6 μmol) at rt under N_2

stream 10 min prior to EOB. [^{11}C]HCN gas was bubbled into the mixture at rt and a flow rate of 400 mL/min until the radioactivity reached saturation. The solution was then heated to 80°C for 2 min. A solution of **21b** (3.3 mg, 7.4 μmol) in DMF (250 μL) was added to the reaction mixture at rt and heated to 165°C for 3 min. Subsequently, it was cooled to 80°C, and TFA (500 μL) was added to the reaction mixture and heated to 80°C for 3 min. The reaction mixture was allowed to cool to rt, then neutralized with 5 M sodium acetate (1.25 mL), and purified on HPLC (Capcell Pak C_{18}, S-5μm, 10 mm ID × 250 mm, Shiseido, Japan) using the mobile phase of CH_3CN/H_2O/TEA (5/5/0.01, v/v/v) at a flow rate of 5.0 mL/min to give 199.4 MBq of [^{11}CN]**21a**. The t_R of [^{11}CN]**21a** was 11.0 min for purification and 5.8 min for analysis on HPLC. The synthesis time from EOB, 35.4 min; radiochemical yield (decay-corrected), 5.8% based on [^{11}C]CO_2; radiochemical purity, > 99%; specific activity at EOS, 61 GBq/μmol.

2-(1-(3-([^{11}C]Methylamino)phenyl)-2-oxo-5-(pyrimidin-2-yl)-1,2-dihydropyridin-3-yl)benzonitrile ([^{11}C]21a). [^{11}C]CH_3OTf was synthesized by a procedure shown in the literature.[38] [^{11}C]CH_3OTf was generated by reaction of the produced [^{11}C]CH_3I with 150–200 mg of silver triflate (fixed on Graphpac GC; quartz glass column; I.D.: 3.9 mm; O.D.: 6 mm; length: 200 mm) in an online flowthrough process at 180°C using a nitrogen gas flow of 50 mL/min.

[^{11}C]CH_3OTf gas was introduced to **20a** (0.50 mg, 1.4 μmol) in dry acetone (250 μL) through bubbling tube at rt until the radioactivity reached saturation, and subsequently the reaction mixture was dried at 80°C under an N_2 stream. The residue was dissolved in HPLC eluent (1 mL), and was purified on HPLC (Capcell Pak C_{18}) using the mobile phase of CH_3CN/H_2O/TEA (4.5/5.5/0.01, v/v/v) at a flow rate of 5.0 mL/min to give [^{11}C]**21a** (1.69 GBq yield at EOS from 21.4 GBq of bombardment at EOB). The synthesis time from EOB, 32.4 min; radiochemical yield (decay-corrected), 23.7% based on [^{11}C]CO_2; radiochemical purity, > 99%; specific activity at EOS, 183 GBq/μmol. In this reaction condition, a trace amount of ^{11}C-labeled dimethylated compound was observed (approximately 1.5% of total radioactivity, t_R of ^{11}C-labeled *N,N*-dimethyl version was eluted for 11.2 min for analysis on HPLC). The spectrum data are noted in Supporting Information, Figure 9.

1-(3-([^{18}F]Fluoromethyl)phenyl)-3-(2-fluorophenyl)-5-(pyrimidin-2-yl)pyridin-2(1*H*)-one ([^{18}F]24a). [^{18}F]F^- was produced by ^{18}O(p,n)^{18}F reaction on 95 atom% $H_2{}^{18}O$ using 18 MeV protons (14.2 MeV on target) from a cyclotron and separated from [^{18}O]H_2O using Dowex 1-X8 anion exchange resin. [^{18}F]F^- was eluted from the resin with an aqueous solution of potassium carbonate (10 mM, 500μL) into a vial containing a solution of Kryptofix 222 (25 mg) in CH_3CN (1.5 mL) and transferred to another

reaction vessel in hot cells. The [^{18}F]F$^-$ solution was dried to remove water and CH_3CN at 120°C for 15 min.

A solution of **24b** (1.5 mg, 2.8 μmol) in anhydrous CH_3CN (300 μL) was added to the reaction vessel containing [^{18}F]F$^-$ and heated at 85°C for 10 min. The reaction mixture was purified on HPLC (YMC, J'Sphere C18, S-5μm, 10 mm ID × 250 mm) using a mobile phase of CH_3CN/water/triethylamine (5.0/5.0/0.01, v/v/v) at a flow rate of 5.0 mL/min to give the title compound (1.24 GBq yield at EOS from 5.00 GBq of bombardment at EOB). The t_R of the title compound was 17.3 min for purification and 6.5 min for analysis on HPLC. The synthesis time from EOB, 70.5 min; radiochemical yield (decay-corrected), 33.8% based on [^{18}F]F$^-$; radiochemical purity, > 99%; specific activity at EOS, 297 GBq/μmol. The analytical HPLC conditions are as follows: column: Capcell Pak C18, S-5μm, 4.6 mm ID × 250 mm; eluent: CH_3CN/water/triethylamine = 6.5/3.5/0.01 (v/v/v); flow rate: 1.0 mL/min; detector: UV-254 nm and RI.

Receptor Binding Assay. Homogenate of forebrains of SD rats was prepared in ice-cold solution containing 0.32 M sucrose and 0.1 mM EGTA (pH 7.4). Homogenate was centrifuged at 1000*g* for 10 min and supernatant was collected. This supernatant was centrifuged at 30,000*g* for 20 min. Precipitate was suspended in 1 mM EGTA/Tris

buffer (pH 8.0) by sonication, subjected to osmotic lysis on ice for 10 min and centrifuged at 30,000*g* for 20 min. This procedure was conducted twice. Precipitate was suspended in 50 mM Tris HCl buffer (pH 7.4) by sonication and centrifuged at 30,000*g* for 20 min. This procedure was conducted three times. Precipitate was suspended in 50 mM Tris HCl buffer (pH 7.4) by sonication and stored at –80°C. On the day of binding assay, the stored solution was suspended in 50 mM Tris HCl buffer (pH 7.4) by sonication and centrifuged at 30,000*g* for 20 min. This procedure was performed three times. Precipitate was suspended in 50 mM Tris-HCl buffer (pH 7.4) by sonication and used for binding assay.

Receptor solution was re-suspended in binding buffer (50 mM Tris-HCl, pH 7.4) to a final concentration of 0.24 mg tissue equivalent/assay. The incubation time for [^{3}H]perampanel on AMPA receptor was 90 min at 4°C. After incubation, membranes were filtered onto GF/B filter presoaked with 0.3% PEI and washed three times with ice–cold wash buffer (same as binding buffer). Each filter was placed in a vial, and 6 mL of liquid scintillator reagent (Hionic-Fluor; PerkinElmer Life & Analytical Sciences, Shelton, CT) were added. Radioactivity was counted (1 min) in a liquid scintillation counter (LSC-6100; Hitachi Aloka Medical, Ltd., Tokyo, Japan). Saturation isotherms were determined by addition of various concentrations of [^{3}H] perampanel (1–2000

nM). Nonspecific bindings for [^{3}H]perampanel were measured in the presence of 15 μM unlabeled compounds. K_D value for [^{3}H]perampanel was calculated by Scatchard analysis of the saturation isotherm experiment. The reaction was then performed in the presence of a test compound at three different concentrations to estimate IC_{50} value for inhibition of [3H]perampanel binding.

Measurement of Lipophilicity. cLogP values of tested compounds were determined computationally using Daylight Software ver. 4.94 (Daylight Chemical Information Systems, Inc., Niguel, CA). LogD values of selected compounds were measured by mixing ^{11}C-labeled compound (radiochemical purity, 100%; about 200,000 cpm) with *n*-octanol (3.0 g) and phosphate buffered saline (PBS; 3.0 g, 0.1 M, pH 7.4) in a test tube. The mixture was vortexed for 3 min at rt, followed by centrifugation at 2330*g* for 5 min. Aliquots of 1 mL of PBS and 1 mL of *n*-octanol were removed and weighed, and their radioactivity was quantified with a 1480 Wizard automatic γ counter (Perkin-Elmer, Waltham, MA). A sample from the remaining organic layer was removed, and repartitioned until a consistent LogD was obtained. The LogD value was calculated by the following formula: LogD = Log[(cpm/g *n*-octanol)/(cpm/g PBS)]. All measurements were performed in triplicate.

P-gp Transcellular Transport Study. P-gp-mediated transfer of tested compounds

was assayed using cell lines as described elsewhere. LLC-PK1 and LLC-MDR1 cells were seeded at a density of 4.0×10^5 cells/cm^2 onto porous membrane filters of 24-well cell culture insert plates. Cells were cultured in 5% CO_2 at 37°C, and were used for the transport studies five days after seeding. For trans-cellular transport experiments, each cell monolayer was pre-incubated at 37°C for 2 h in Hank's balanced salt solution containing 10 mM HEPES (HBSS buffer).

Trans-cellular transport experiments were initiated by adding the solution of test compounds to the apical or basal side of the cell culture inserts. After incubation at 37°C for 2 h, HBSS buffer was sampled from the opposite compartment of that spiked with test compounds, and the test compound concentration in the sample was measured by LC–MS.

The apparent permeability coefficient (P_{app}) of the test compounds was estimated using the following Equation 1, where Q, t, C_0, and A represent permeated amount of test compounds, incubation time, initial concentration of test compounds, and membrane area, respectively:

$$P_{app} = Q/t/C_0/A \qquad (1)$$

FRs across the monolayer of LLC-PK1 and LLC-MDR1 were defined according to the following Equation 2, where $P_{app,\ b\ to\ a}$ and $P_{app,\ a\ to\ b}$ represent the P_{app} in the

basal-to-apical and apical-to-basal directions, respectively, and the corrected FR was defined by Equation 3:

$$FR = P_{app,\ b\ to\ a} \ / \ P_{app,\ a\ to\ b} \qquad (2)$$

$$\text{Corrected FR} = (\text{FR in LLC-MDR1 cells}) / (\text{FR in LLC-PK1 cells}) \qquad (3)$$

Animals. Wild-type mice (FVB) at 12–14 weeks of age (male, 30–32 g) and P-gp/BCRP double-knockout mice (Abcb1a/1b$^{-/-}$Abcg2$^{-/-}$) at 18–19 weeks of age (male, 32–34 g) purchased from Taconic Farm (Hudson, NY) were used.

SD rats at 9–11 weeks of age (male, 410–500 g) were purchased from Japan SLC (Shizuoka, Japan), and P-gp–knockout rats at 10 weeks of age (Mdr1a knockout rats, male, 410–500 g) were purchased from SAGE Labs (St. Louis, MO). The animals were housed under a 12 h light–dark cycle, allowed free access to food pellets and water, and used for in vivo PET studies. Two rhesus monkeys (*Macaca mulatta*) at 3 years and 8 months of age (male, weighing 4.25 kg and 4.50 kg, respectively) were purchased from Japan SLC. The monkeys were housed in individual cages and were given a balanced diet and *ad libitum* tap water from a feeding valve. The room was illuminated from 7 a.m. to 9 p.m. The monkeys at the time of PET scanning were 3 years and 11 months old and their weight ranged between 5 and 6 kg. The animal experiments were approved

by the Committee for the Care and Use of Laboratory Animals of the National Institute of Radiological Sciences (NIRS).

Cassette Dosing. Each of 12 test compounds was dissolved in DMSO at a concentration of 10 mg/mL. Identical volumes of four solutions were mixed and diluted with distilled water to obtain the dosing solution for cassette administration (0.05 mg/mL of each compound). The dosing solution was administered intravenously into a rat at 0.05 mg/kg per compound (1 mL/kg). Rat blood and brain were collected at 5, 30, and 60 min (n = 2 for each time point). Animals were anesthetized with isoflurane prior to sacrifice. Whole blood was collected into a heparinized syringe from abdominal aorta and plasma was separated by centrifugation. Following blood collection, whole brains were collected by decapitation, rinsed in saline, and weighed. Brain tissues were homogenized with a tissue homogenizer (Hiscotron, Microtec Co., Ltd., Chiba, Japan) in 4 volumes of distillated water (20% homogenate). Fifty microliter aliquots of plasma and brain homogenate samples were dispensed into tubes and 200 μL of CH_3CN containing internal standard (tamsulosin hydrochloride) was added to each tube. The sample was then vortexed vigorously and centrifuged at 3000 rpm for 10 min at 4°C (Model 5930, Kubota Corporation, Tokyo, Japan). After centrifugation, 200 μL of the supernatant was transferred to a 96-well filter plate (MultiScreen Solvinert, Millipore)

and centrifuged at 2000 rpm for 5 min at 4°C. Five microliters of each filtered sample was injected into the HPLC-MS/MS system (HPLC: Alliance 2795, Waters, Watford, UK, MS/MS: Quattro Ultima-Pt; Micromass, Manchester, UK).

In Vitro Autoradiography. Rat and monkey brain sections (20-μm thickness) were dried at rt and pre-incubated for 20 min in 50 mM Tris-HCl buffer (pH 7.4) containing 2.5 mM calcium chloride at 4°C. After pre-incubation, these sections were incubated for 60 min at 4°C in fresh buffer with appropriate concentrations of the compounds (1-160 nM). Unlabeled compounds (10 μM) were used to assess nonspecific binding of these radioligands in the brain. After incubation, brain sections were rapidly washed three times with solution equivalent to the incubation buffer, and were blow-dried. An imaging plate (BAS-IP MS2025, Fujifilm, Tokyo, Japan) was exposed to the dried sections for 1 h. Radioactive standards calibrated with known amounts of the labeled compounds were incorporated into the exposure process. Autoradiograms were generated and displayed using a computer-assisted image analyzer (Multi Gauge; Fujifilm).

Ex Vivo Receptor Occupancy Study in Rats. Fifteen min after intravenous injection of [^{11}C]**21a**, five rats (male SD at 12 weeks of age) were killed by decapitation. Among these animals, three rats were treated with oral administration of **10** (10 mg/kg

in 0.5% methyl cellulose suspension) 45 min prior to [^{11}C]**21a** injection. The injected dose and mass of [^{11}C]**21a** was 370 ± 50 MBq and 3.3 ± 0.5 nmol/kg, respectively. Blood and whole brain were removed quickly and the blood sample (0.5 mL) was centrifuged at 20 000*g* for 2 min at 4°C to separate plasma. The supernatant (0.2 mL) was then collected in a test tube, and stored at –20°C. Plasma concentration of perampanel was determined by LC-MS. The plasma analyses were performed under blind conditions after all imaging analyses were completed to prevent bias. Coronal brain slices (2 mm thickness) were prepared by brain slicer (BRM4000C; BioResearchCenter), and the brain sections (CTX and BS level) were placed on a micro slide glass, surrounded by a handmade silicon device with equalthickness to protect the brain slices, and exposed to an imaging plate (BAS-TR2025; Fujifilm Co.) for 1 h. Quantitative autoradiographic analysis was performed using a computer-assisted image analyzer (Multi Gauge; Fujifilm). Optical density values were converted to fmol/mg protein by regression analysis with the radioactive standards.

Rodent PET studies. Prior to PET scans, anatomical template images of the mouse and rat brains were generated by a high-resolution MRI system following the procedure described in the literature.[33] PET scans of anesthetized rats and mice were performed with a small animal-dedicated micro-PET FOCUS 220 system (Siemens Medical

Solutions, Malvern, PA), which yields a 25.8 cm (transaxial) × 7.6 cm (axial) FOV, and a spatial resolution of 1.3 mm full-width at half-maximum (FWHM) at the center of the FOV. Subsequently, list-mode scans were performed for 90 min. All list-mode data were sorted and Fourier-rebinned into 2-dimensional sinograms (frames, 1 min × 4 scans, 2 min × 8 scans, 5 min × 14 scans). After that, images were reconstructed using 2-dimensional filtered back-projection with a 0.5-mm Hanning filter. To inject radioligand solution, a 24-gauge needle with catheter (Terumo, Tokyo, Japan) was placed into the rat tail vein. The injected dose of the radioligand was 78.7–189.8 MBq (127.6 ± 43.1 MBq, 1.3 ± 0.4 nmol, mean ± SD). Body temperature was maintained at 37°C in rats and 40°C in mice with a plate heater (Bio Research Center Inc., Aichi, Japan). During the scan, the animals were kept anesthetized with 1.5% (v/v) isoflurane.

Monkey PET studies. Prior to the PET scans, MRI of each monkey brain was obtained using EXCELART/VG Pianissimo 1.0 tesla (Toshiba, Japan) and three-dimensional field echo sequence (repetition time = 14 ms, echo time = 6.8 ms, flip angle 20°, FOV = 120 mm, number of slices = 60, slice thickness = 1 mm without slice gap, 128 × 128 acquisition matrix, which after reconstruction was reformatted to a 256 × 256 image matrix, number of excitations = 2, acquisition time = 3 min 57 s). During MR scanning, monkeys were anesthetized with continuous intravenous infusion of

propofol (0.2–0.6 mg/kg/min). PET scans of a monkey were performed using a high-resolution SHR-7700 PET camera (Hamamatsu Photonics, Shizuoka, Japan) designed for laboratory animals, which provides 31 transaxial slices 3.6 mm (center-to-center) apart and a 33.1 cm (transaxial) ×11.16 cm (axial) FOV. Spatial resolution for the reconstructed images was 2.6 mm FWHM at the center of the FOV. Prior to the PET scans, the monkey was initially anesthetized with thiamylal (15 mg/kg, i.v.), and anesthesia was maintained using 1.0–2.0% (v/v) isoflurane. Following a transmission scan for attenuation correction using a ^{68}Ge–^{68}Ga source, dynamic emission scans were conducted in a 3-dimensional acquisition mode for 90 min (frames, 1 min × 4 scans, 2 min × 8 scans, 5 min × 14 scans). Emission scan data were reconstructed with a 4-mm Colsher filter. A radioligand was injected via the crural vein as a single bolus upon initiation of emission scans. The injected dose of the radioligand was approximate 110 MBq (1.0 nmol)/monkey. For a blocking PET study, unlabeled compound (**21a)** at doses of 0.02, 0.05, and 0.1 mg/kg formulated in 5 mL of saline with 10% DMSO was intravenously administered via the crural vein as a single slow bolus over 10 min, at 15 min prior to radioligand administration. Baseline and blocking PET scans were performed for the same two monkeys.

PET data analysis. Anatomical regions of interest were manually defined on CTX, HIP, BS and several other areas in MRI images co-registered with PET data using PMOD® software (PMOD Technologies Ltd., Zurich, Switzerland), as exemplified in Supporting Information, Figure 10. Regional radioactivity in the brain was expressed as the percent of injected dose per unit tissue volume (% ID/mL) in the rat experiments, and as the percentage standardized uptake value [% SUV = % ID/mL × body weight (g)] in the monkey experiments.

Off-target Binding Assay. Binding of **21a** to an off-target binding component was measured as a percent inhibition of control specific binding in the presence of **21a** as follows:

$$100 - \left(\frac{\text{measured specific binding}}{\text{control specific binding}} \times 100\right)$$

The IC_{50} values (concentration causing half-maximal inhibition of control specific binding) and Hill coefficients (nH) were determined by non-linear regression analysis of the competition curves generated with mean replicate values using Hill equation curve fitting by the following equation:

$$Y = D + \left[\frac{A - D}{1 + (C / C_{50})^{nH}}\right]$$

where Y = specific binding, A = left asymptote of the curve, D = right asymptote of the curve, C = compound concentration, C_{50} = IC_{50}, and nH = slope factor. This analysis

was performed using software developed at Cerep (Hill software), and validated by comparison with data generated by the commercial software SigmaPlot® 4.0 for Windows® (© 1997 by SPSS Inc.). The inhibition constants (K_i) were calculated using the Cheng Prusoff equation as shown below:

$$K_{\mathrm{i}} = \frac{\mathrm{IC}_{50}}{(1 + \mathrm{L} / K_{\mathrm{D}})}$$

where L = concentration of the radioligand in the assay, and K_D = affinity of the radioligand for the receptor predetermined by a Scatchard plot analysis using various concentrations of the radioligand..

ASSOCIATED CONTENT

Supporting Information

Figure 1: Workflow for selection of PET probe candidates. Figure 2: Rat PET study of [^{11}C]**19a**. Figure 3: Mouse PET study of [^{11}C]**20a**. Figure 4: In vitro autoradiographic labeling of monkey brain sections with [^{11}C]**20a**–**23a**. Figure 5: Rat PET study of [^{11}C]**22a**. Figure 6: Rat PET study of [^{11}C]**23a**. Figure 7: Rat PET study of [^{11}C]**24a**. Figure 8: Synthesis, spectrum data, and HPLC charts of unlabeled compounds. Figure 9: Radiosynthesis, HPLC charts on purification, and HPLC charts of the formulated sample. Figure 10: Definition of regions of interest in rat and monkey brain images.

Table 1: Assays of Off-target Binding of **21a**.

This material is available free of charge via the internet at http://pubs.acs.org.

AUTHOR INFORMATION

Corresponding Author

Makoto Higuchi, M. D., Ph. D.

*Phone: +81 43 206 4700. Fax: +81 43 253 0396. E-mail: mhiguchi@nirs.go.jp.

Address: Molecular Imaging Center, National Institute of Radiological Sciences, 4-9-1 Anagawa, Inage-ku, Chiba, Chiba 263-8555, Japan.

Notes

The authors declare no competing financial interest.

ACKNOWLEDGEMENTS

The authors are grateful to the staff of NIRS and Eisai for support with the cyclotron operation, radioisotope production, radiosynthesis, and animal experiments, and especially thank Mr. Yuichiro Yoshida, Mr. Masanao Ogawa, and Mr. Nobuki Nengaki

for manipulating the semi-auto synthetic machine in hot cells; Dr. Mitsuaki Ino, Dr. Katsutoshi Ido and Dr. Takahisa Hanada for pharmacological support; Mr. Kenji Furutsuka for HRMS; Mr. Takashi Okauchi, Ms. Kaori Yamada, and Ms. Syoko Uchida for rat PET scans; Dr. Francois Bernier, Dr. Krause Stephen, and Dr. Paul McCracken for their assistance in the preparation of the manuscript; Dr. Teiji Kimura, Dr. Takayuki Hida, Dr. Makoto Ogo, and Dr. Kumiko Saegusa for research program management. This work was supported in part by a Grant-in-Aid for Scientific Research on Innovative Areas ("Brain Environment") 23111009 (M. H.) from the Ministry of Education, Culture, Sports, Science and Technology, Japan.

ABBREVIATIONS USED

A_{2A}, adenosine 2A receptor; AcOEt, ethyl acetate; BAST, bis(2-methoxymethyl)aminosulfur trifluoride; BCRP, breast cancer resistance protein; BS, brain stem; CDI, carbodiimidazole; CER, cerebellum; CTX, cerebral cortex; EOB, end of bombardment; EOS, end of synthesis; FR, flux ratio; HIP, hippocampus; % ID, per unit tissue volume; Kryptofix 222, 4,7,13,16,21,24-hexaoxa-1,10-diazabicyclo[8,8,8]hexacosane; pBZR, peripheral benzodiazepine receptor; SD rat, Sprague Dawley rat; % SUV, percentage standardized uptake value; TACs, time–radioactivity curves; transmembrane AMPA receptor

regulartory protein, TARP; TEA, triethylamine; THA, thalamus; t_R, retention time.

REFERENCES

(1) Meldrum, B. S. Glutamate as a neurotransmitter in the brain: review of physiology and pathology. *J. Nutr.* **2000**, *130*, 1007S-1015S.

(2) Mayer, M. L.; Armstrong, N. Structure and function of glutamate receptor ion channels. *Annu. Rev. Physiol.* **2004**, *66*, 161-181.

(3) Watkins, J. C.; Jane, D. E. The glutamate story. *Br. J. Pharmacol.* **2006,** *147 (Suppl. 1)*, S100-S108.

(4) Niswender, C. M.; Conn, P. J. Metabotropic glutamate receptors: physiology, pharmacology, and disease. *Annu. Rev. Pharmacol. Toxicol.* **2010**, *50*, 295-322.

(5) Asztely, F.; Gustafsson, B. Ionotropic glutamate receptors. Their possible role in the expression of hippocampal synaptic plasticity. *Mol. Neurobiol*. **1996**, *12*, 1-11.

(6) Calabresi, P.; Cupini L. M.; Centonze, D.; Pisani, F.; Bernardi G. Antiepileptic drugs as a possible neuroprotective strategy in brain ischemia. *Ann. Neurol.* **2003**, *53*, 693-702.

(7) Chang, P. K.; Verbich, D.; McKinney, R. A. AMPA receptors as drug targets in neurological disease-advantages, caveats, and future outlook. *Eur. J. Neurosci.* **2012**, *35*,

1908-1916.

(8) Meldrum, B. S.; Rogawski, M. A. Molecular targets for antiepileptic drug development. *Neurotherapeutics* **2007**, *4*, 18-61.

(9) Turski, L.; Huth, A.; Sheardown, M.; McDonald, F.; Neuhaus, R.; Schneider, H. H.; Dirnagl, U.; Wiegand, F.; Jacobsen, P.; Ottow, E. ZK200775: a phosphonate quinoxalinedione AMPA antagonist for neuroprotection in stroke and trauma. *Proc. Natl. Acad. Sci. U.S.A.* **1998**, *95*, 10960-10965.

(10) Ornstein, P. L.; Arnold, M. B.; Augenstein, N. K.; Lodge, D.; Leander, J. D.; Schoepp, D. D. (3*SR*,4a*RS*,6*RS*,8a*RS*)-6-[2-(1*H*-tetrazol-5-yl)ethyl]decahydroisoquinoline-3-carboxylic acid: a structurally novel, systemically active, competitive AMPA receptor antagonist. *J. Med. Chem.* **1993**, *36*, 2046-2048.

(11) Gilron, I.; Max, M. B.; Lee, G.; Booher, S. L.; Sang, C. N.; Chappell, A. S.; Dionne, R. A. Effects of the 2-amino-3-hydroxy-5-methyl-4-isoxazole-proprionic acid/kainate antagonist LY293558 on spontaneous and evoked postoperative pain. *Clin Pharmacol. Ther.* **2000**, *68*, 320-327.

(12) Faught, E. BGG492 (selurampanel), an AMPA/kainate receptor antagonist drug for epilepsy. *Expert Opin. Invest. Drugs* **2014**, *23*, 107-113.

(13) De Sarro, G.; Gitto, R.; Russo, E.; Ibbadu, G. F.; Barreca, M. L.; De Luca, L.;

Chimirri, A. AMPA receptor antagonists as potential anticonvulsant drugs. *Curr. Top. Med. Chem.* **2005**, *5*, 31-42.

(14) Donevan, S. D.; Yamaguchi, S.; Rogawski, M. A. Non-*N*-methyl-D-aspartate receptor antagonism by 3-*N*-substituted-2,3-benzodiazepines: relationship to anticonvulsant activity. *J. Pharmacol. Exp. Ther.* **1994**, *271*, 25-29.

(15) Chappell, A. S.; Sander, J. W.; Brodie, M. J.; Chadwick, D.; Lledo, A.; Zhang, D. Bjerke, J.; Kiesler, G. M.; Arroyo S. A crossover, add-on trial of talampanel in patients with refractory partial seizures. *Neurology* **2002**, *58*, 1680-1682.

(16) Menniti, F. S.; Buchan, A. M.; Chenard, B. L.; Critchett, D. J.; Ganong, A. H.; Guanowsky, V.; Seymour, P. A.; Welch, W. M. CP-465,022, a selective noncompetitive AMPA receptor antagonist, blocks AMPA receptors but is not neuroprotective in vivo. *Stroke* **2003**, *34*, 171-176.

(17) Yamashita, H.; Ohno, K.; Amada, Y.; Hattori, H.; Ozawa-Funatsu, Y.; Toya, T.; Inami, H.; Shishikura, J.; Sakamoto, S.; Okada, M.; Yamaguchi, T. Effects of 2-[*N*-(4-chlorophenyl)-*N*-methylamino]-4*H*-pyrido[3.2-e]-1,3-thiazin-4-one (YM928), an orally active alpha-amino-3-hydroxy-5-methyl-4-isoxazolepropionic acid receptor antagonist, in models of generalized epileptic seizure in mice and rats. *J. Pharmacol. Exp. Ther.* **2004**, *308*, 127-133.

(18) Feigin, V. Irampanel Boehringer Ingelheim. *Curr. Opin. Invest. Drugs* **2002**, *3*, 908-910.

(19) French, J. A.; Krauss, G. L.; Steinhoff, B. J.; Squillacote, D.; Yang, H.; Kumar, D.; Laurenza, A. Evaluation of adjunctive perampanel in patients with refractory partial-onset seizures: results of randomized global phase III study 305. *Epilepsia* **2013**, *54*, 117-125.

(20) Meyer, J. H.; Wilson, A. A.; Sagrati, S.; Hussey, D.; Carella, A.; Potter, W. Z.; Ginovart, N.; Spencer, E. P.; Cheok, A.; Houle, S. Serotonin transporter occupancy of five selective serotonin reuptake inhibitors at different doses: an [^{11}C]DASB positron emission tomography study. *Am. J. Psychiatry* **2004**, 161, 826-835.

(21) Sato, H.; Ito, C.; Tashiro, M.; Hiraoka, K.; Shibuya, K.; Funaki, Y.; Iwata, R.; Matsuoka, H.; Yanai, K. Histamine H_1 receptor occupancy by the new-generation antidepressants fluvoxamine and mirtazapine: a positron emission tomography study in healthy volunteers. *Psychopharmacology* **2013**, *230*, 227-234.

(22) Arakawa, R.; Ito, H.; Takano, A.; Takahashi, H.; Morimoto, T.; Sassa, T.; Ohta, K.; Kato, M.; Okubo, Y.; Suhara, T. Dose-finding study of paliperidone ER based on striatal and extrastriatal dopamine D2 receptor occupancy in patients with schizophrenia. *Psychopharmacology* **2008**, *197*, 229-235.

(23) Arstad, E.; Gitto, R.; Chimirri, A.; Caruso, R.; Constanti, A.; Turton, D.; Hume S. P.; Ahmad, R.; Pilowsky, L. S.; Luthra, S. K. Closing in on the AMPA receptor: Synthesis and evaluation of 2-acetyl-1-(4'-chlorophenyl)-6-methoxy-7-[^{11}C]methoxy-1,2,3,4-tetrahydroisoquinoline as a potential PET tracer. *Bioorg. Med. Chem. Lett.* **2006**, *14*, 4712-4717.

(24) Gao, M.; Kong, D.; Clearfield, A.; Zheng, Qi-Huang. *N*-acetyl-1-aryl-6,7-dimethoxy-1,2,3,4-tetrahydroisoquinoline derivatives as new potential PET AMPA receptor ligands. Synthesis of carbon-11 and fluorine-18 labeled *Bioorg. Med. Chem. Lett.* **2006**, *16*, 2229-2233.

(25) Andrasi, F. Production of molecules suitable for early diagnosis of Alzheimer disease. HU 2011/000111, October 29, 2012.

(26) Lee H. G.; Milner, P. J.; Placzek, M. S.; Buchwald, S. L.; Hooker, J. M. Virtually instantaneous, room-temperature [^{11}C]-cyanation using biaryl phosphine Pd(0) complexes. *J. Am. Chem. Soc*. **2015**, *137*, 648-651.

(27) Kato, A.S.; Gill, M. B.; Yu, H.; Nisenbaum, E. S.; Bredt, D. S. TARPs differentially decorate AMPA receptors to specify neuropharmacology. *Trends Neurosci.* **2010**, *33*, 241-248.

(28) Schober, D. A.; Gill, M. B.; Yu, H.; Gernert, D. L.; Jeffries, M. W.; Ornstein, P. L.; Kato, A. S.; Felder, C. C.; Bredt, D. S. Transmembrane AMPA receptor regulatory proteins and cornichon-2 allosterically regulate AMPA receptor antagonists and potentiators. *J. Biol. Chem.* **2011**, *286*, 13134-13142.

(29) Nagato, S.; Ueno, K.; Kawano, K.; Norimine, Y.; Ito, K.; Hanada; T.; Ueno, M.; Amino, H.; Ohgoh, M.; Hatakeyama, S.; Urawa, Y.; Naka, H.; Groom, A. J.; Rivers, L.; Smith, T. 1,2-Dihidropyridine compounds, process for preparation of the same and use thereof. WO2001/96308, June 8, 2001.

(30) Hibi, S.; Ueno, K.; Nagato, S.; Kawano, K.; Ito, K.; Norimine, Y.; Takenaka, O.; Hanada, T.; Yonaga, M. Discovery of 2 - (2-Oxo-1-phenyl-5-pyridin-2-yl-1,2-dihydropyridin-3-yl)benzonitrile (perampanel): A novel, noncompetitive α-amino-3-hydroxy-5-methyl-4-isoxazolepropanoic acid (AMPA) receptor antagonist. *J. Med. Chem.* **2012**, *55*, 10584-10600.

(31) Nagato, S.; Kawano, K.; Ito, K.; Norimine, Y.; Ueno, K.; Hanada; T.; Amino, H.; Ogo, M.; Hatakeyama, S.; Ueno, M.; Groom, A. J.; Rivers, L.; Smith, T. Pyridazinones and triazinones and medical use thereof. WO2002/22587, September 17, 2001.

(32) Nagilla, R.; Nord, M.; McAtee, J. J.; Jolivette, L. J. Cassette dosing for pharmacokinetic screening in drug discovery: comparison of clearance, volume of

distribution, half-life, mean residence time, and oral bioavailability obtained by cassette and discrete dosing in rats. *J. Pharm. Sci.* **2011**, *100*, 3862-3874.

(33) Oi, N.; Suzuki, M.; Terauchi, T.; Tokunaga, M.; Nakatani, Y.; Yamamoto, N.; Fukumura, T.; Zhang, M. –R.; Suhara, T.; Higuchi, M. Synthesis and evaluation of novel radioligands for positron emission tomography imaging of orexin-2 receptor. *J. Med. Chem.* **2013**, *56*, 6371-6385.

(34) Zhang, L.; Villalobos, A.; Beck, E. M.; Bocan, T.; Chappie, T. A.; Chen, L.; Grimwood, S.; Heck, S. D.; Helal, C. J.; Hou, X.; Humphrey, J. M.; Lu, J.; Skaddan, M. B.; McCarthy, T. J.; Verhoest, P. R.; Wager, T. T.; Zasadny, K. Design and selection parameters to accelerate the discovery of novel central nervous system positron emission tomography (PET) ligands and their application in the development of a novel phosphodiesterase 2A PET ligand. *J. Med. Chem.* **2013**, *56*, 4568-4579.

(35) Iwata, R.; Ido, T.; Takahashi, T.; Nakanishi, H.; Iida, S. Optimization of [^{11}C]HCN production and no-carrier-added [1-^{11}C]amino acid synthesis. *Int. J. Rad. Appl. Instrum. A.* **1987**, *38*, 97-102.

(36) Fujinaga, M.; Yamasaki, T.; Kawamura, K.; Kumata, K.; Hatori, A.; Yui, J.; Yanamoto, K.; Yoshida, Y.; Ogawa, M.; Nengaki, N.; Maeda, J.; Fukumura, T.; Zhang, M. -R. Synthesis and evaluation of

6-[1-(2-[^{18}F]fluoro-3-pyridyl)-5-methyl-1*H*-1,2,3-triazol-4-yl]quinoline for positron emission tomography imaging of the metabotropic glutamate receptor type 1 in brain. *Bioorg. Med. Chem.* **2011**, *19*, 102-110.

(37) Oi, N.; Yamamoto, N.; Suzuki, M.; Nakatani, Y.; Suhara, T.; Zhang, M. –R.; Fukumura, T.; Higuchi, M.; Minamimoto, T.; Maeda, J.; Tokunaga, M.; Nagai, Y. [^{11}C] and [^{18}F] labeled 1,3-diphenyl-5-(pyrimidin-2-yl)-pyridin-2(1*H*)-one derivatives and their use for PET imaging of the AMPA receptor. WO2014/163210, April 2, 2014.

(38) Holschbach, M.; Schüller, M. An on-line method for the preparation of n.c.a. [$^{11}CH_3$]trifluoromethanesulfonic acid methyl ester. *Appl. Radiat. Isot.* **1993**, *44,* 897-898.

(39) Hanada T.; Hashizume, Y.; Tokuhara, N.; Takenaka, O.; Kohmura, N.; Ogasawara, A.; Hatakeyama, S.; Ohgoh, M.; Ueno, M.; Nishizawa, Y. Perampanel: a novel, orally active, noncompetitive AMPA-receptor antagonist that reduces seizure activity in rodent models of epilepsy. *Epilepsia* **2011**, *52*, 1331-1340.

(40) Gidal, B. E.; Ferry, J.; Majid, O.; Hussein, Z. Concentration-effect relationships with perampanel in patients with pharmacoresistant partial-onset seizures. *Epilepsia* **2013**, *54*, 1490-1497.

(41) Papadopoulos V. Peripheral benzodiazepine receptor: structure and function in

health and disease. *Ann. Pharm. Fr.* **2003**, *61*, 30-50.

(42) Luthin, D. R.; Lee, K. S.; Okonkwo, D.; Zhang, P.; Linden, J. Photoaffinity labeling with 2(-)[2-(4-azido-3(-)[^{125}I]-iodophenyl)ethylamino]adenosine and autoradiography with 2(-)[2-(4-amino-3(-)[^{125}I]iodophenyl)ethylamino]adenosine of A_{2a} adenosine receptors in rat brain. *J. Neurochem.* **1995**, *65*, 2072-2079.

(43) Brooks, B. J.; Doder, M.; Osman, S.; Luthra, S. K.; Hirani, E.; Hume, S.; Kase, H.; Kilborn, J.; Martindill, S.; Mori, A. Positron emission tomography analysis of [^{11}C]KW-6002 binding to human and rat adenosine A_{2A} receptors in the brain. *Synapse* **2008**, *62*, 671-681.

(44) Pike, V. W.; Rash, K. S; Chen, Z.; Pedregal, C.; Statnick, M. A.; Kimura, Y.; Hong, J.; Zoghbi, S. S.; Fujita, M.; Toledo, M. A.; Diaz, N.; Gackenheimer, S. L.; Tauscher, J. T.; Barth, V. N.; Innis, R. B. Synthesis and evaluation of radioligands for imaging brain nociceptin/orphanin FQ peptide (NOP) receptors with positron emission tomography. *J. Med. Chem.* **2011**, *54*, 2687-2700.

(45) Pedregal, C.; Joshi, E. M.; Toledo, M. A.; Lafuente, C.; Diaz, N.; Martinez-Grau M. A.; Jiménez, A.; Benito, A.; Navarro, A.; Chen, Z.; Mudra, D. R.; Kahl, S. D.; Rash, K. S.; Statnick, M. A.; Barth, V. N. Development of LC-MS/MS-based receptor

occupancy tracers and positron emission tomography radioligands for the nociceptin/orphanin FQ (NOP) receptor. *J. Med. Chem.* **2012**, *55*, 4955-4967.

Table of Contents/Abstract Graphic